HHS Public Access

Author manuscript

Nat Med. Author manuscript; available in PMC 2022 June 06.

Published in final edited form as:

Nat Med. 2019 November ; 25(11): 1691–1698. doi:10.1038/s41591-019-0635-8.

Generation of functional lungs via conditional blastocyst complementation using pluripotent stem cells

Munemasa Mori[1,8,*], **Kazuhiro Furuhashi**[2], **Jennifer A. Danielsson**[3], **Yuichi Hirata**[2], **Miwako Kakiuchi**[2], **Chyuan-Sheng Lin**[4], **Mayu Ohta**[1], **Paul Riccio**[1], **Yusuke Takahashi**[5,6], **Xinjing Xu**[7], **Charles W. Emala**[3], **Chao Lu**[7], **Hiromitsu Nakauchi**[5,6,8,*], **Wellington V. Cardoso**[1,7,8,*]

[1]Columbia Center for Human Development and Division of Pulmonary, Allergy, Critical Care, Department of Medicine, Columbia University Irving Medical Center, New York, NY, USA.

[2]Columbia Center for Translational Immunology, Department of Medicine, Columbia University Irving Medical Center, New York, NY, USA.

[3]Department of Anethesiology, Columbia University Irving Medical Center, New York, NY, USA.

[4]Bernard and Shirlee Brown Glaucoma Laboratory, Department of Pathology and Cell Biology, College of Physicians and Surgeons, Columbia University Irving Medical Center, New York, NY, USA.

[5]Institute for Stem Cell Biology and Regenerative Medicine, Department of Genetics, Stanford University School of Medicine, Stanford, CA, USA.

[6]Division of Stem Cell Therapy, Distinguished Professor Unit, The Institute of Medical Science, The University of Tokyo, Minato-ku, Tokyo, Japan.

[7]Department of Genetics and Development and Herbert Irving Comprehensive Cancer Center, Columbia University Irving Medical Center, New York, NY, USA.

[8]These authors contributed equally: Munemasa Mori, Hiromitsu Nakauchi, Wellington V. Cardoso.

[*] mm4452@cumc.columbia.edu; nakauchi@stanford.edu; wvc2104@cumc.columbia.edu **Correspondence and requests for materials** should be addressed to M.M., H.N. or W.V.C.

Author contributions

M.M. designed and conducted all experiments; J.A.D. and C.W.E. performed pulmonary function assessment; C.-S.L. and Y.T. supported and performed microinjection and embryo transfer; M.M., P.R. and M.O. maintained mutant mice for the injection; K.F. supported imaging of whole-mount staining; K.F., Y.H., M.O. and M.K. supported and performed hematopoietic cell-colony-formation assay; X.X. and C.L. performed epigenetic experiments; M.M., C.L. and W.V.C wrote the paper; H.N. gave crucial insights on the experiments and the manuscript.

Online content

Any methods, additional references, Nature Research reporting summaries, source data, extended data, supplementary information, acknowledgements, peer review information, details of author contributions and competing interests, and statements of data and code availability are available at https://doi.org/10.1038/s41591019-0635-8.

Competing interests

The authors declare no competing interests.

Additional information

Extended data is available for this paper at https://doi.org/10.1038/s41591-019-0635-8.

Supplementary information is available for this paper at https://doi.org/10.1038/s41591-019-0635-8.

Peer review information Michael Basson was the primary editor on this article and managed its editorial process and peer review in collaboration with the rest of the editorial team.

Reprints and permissions information is available at www.nature.com/reprints.

Abstract

Millions of people worldwide with incurable end-stage lung disease die because of inadequate treatment options and limited availability of donor organs for lung transplantation[1]. Current bioengineering strategies to regenerate the lung have not been able to replicate its extraordinary cellular diversity and complex three-dimensional arrangement, which are indispensable for life-sustaining gas exchange[2,3]. Here we report the successful generation of functional lungs in mice through a conditional blastocyst complementation (CBC) approach that vacates a specific niche in chimeric hosts and allows for initiation of organogenesis by donor mouse pluripotent stem cells (PSCs). We show that wild-type donor PSCs rescued lung formation in genetically defective recipient mouse embryos unable to specify (due to *Ctnnb1*^{cnull} mutation) or expand (due to *Fgfr2*^{cnull} mutation) early respiratory endodermal progenitors. Rescued neonates survived into adulthood and had lungs functionally indistinguishable from those of wild-type littermates. Efficient chimera formation and lung complementation required newly developed culture conditions that maintained the developmental potential of the donor PSCs and were associated with global DNA hypomethylation and increased H4 histone acetylation. These results pave the way for the development of new strategies for generating lungs in large animals to enable modeling of human lung disease as well as cell-based therapeutic interventions[4–6].

Nearly 12 million adults in the United States, or 5% of the population, have been diagnosed with chronic obstructive pulmonary disease, and about 180,000 patients die annually with end-stage refractory lung diseases[1]. The only option currently available is lung transplantation, and patients die nearly every day without ever receiving this treatment because of the scarcity of donor organs[7]. Bioengineering approaches for lung regeneration using endogenous progenitors or human PSCs in decellularized scaffolds emerged as promising options[2,8–11]. However, modeling the structural and functional complexities of the lung in vitro has been insurmountably challenging given its extraordinary cellular diversity, with more than 40 cell types from all embryonic layers, and its complex threedimensional (3D) architecture that demands precise alignment of the epithelial and vascular components to form nearly 480 million alveoli for efficient gas exchange[12,13]. Lastly, maintaining tissue integrity and homeostasis in the presence of the continuous periodic changes in mechanical forces by breathing movement and by the high blood-flow output in the vascular compartment represents a major bioengineering problem to overcome[8,9]. We posited that the generation of a functional lung as a platform for regenerative purposes could be achieved if these challenges were bypassed by modeling lung organogenesis in vivo. Thus, we explored the possibility of generating lungs in chimeric animals from donor PSCs using a blastocyst complementation (BC)-based approach[14–16].

Exogenous PSCs injected into an embryo at the blastocyst stage can join in the recipient's developmental program and compete with the host's cells for a niche. Donor cells can take over a particular progenitor defective niche made vacant by inactivation of a gene that is crucial for the initiation of the developmental program of that organ in the host. BC has been used successfully to generate a PSC-derived pancreas and to rescue the neonatal lethality of Pancreatic and Duodenal homeobox 1 (PDX1)-deficient embryos. Although innovative, BC remained challenging, as it often did not result in postnatal survival[17,18]. Gene deletion, when systemic, could lead to defects in multiple organs not rescued by

the donor cells[17]. Moreover, successful BC requires the maintenance of donor PSC's pluripotency and the ability to form chimeras[5]. The PSC must reach the targeted organ niche and faithfully respond to the specific cues of that organogenesis program. Thus, we sought to identify strategies to overcome these issues in the host and donor to allow lung formation. Lung organogenesis initiates when trachea and lung progenitors are collectively specified in the foregut endoderm by Wnt-β-catenin (Ctnnb1) activation[19,20]. Subsequent endodermal activation of fibroblast growth factor receptor 2 (Fgfr2) by local fibroblast growth factor 10 (Fgf10) from the foregut mesoderm is required to selectively expand these lung progenitors to form the primordial lung[21]. Indeed, genetic disruption of *Fgfr2* in mice does not prevent tracheal formation but results in lung agenesis[21,22]. Although it is an attractive option for lung BC modeling, systemic *Fgfr2* deletion was problematic because of lethality by impaired trophoblast formation or later due to multiple defects, including limb agenesis[21–23].

To prevent undesired non-lung phenotypes in the host, we devised a conditional gene-ablation strategy using a lineage-specific promoter to vacate a specific niche in the host endoderm for complementation, named conditional blastocyst complementation (CBC). The CBC then should target an endoderm-derived lineage for which the gene of choice has a crucial non-redundant function, independent of its expression in other organs. We tested this concept by generating mice in which *Fgfr2* was conditionally deleted in the foregut endoderm immediately before the onset of lung organogenesis (*Shh*$^{cre/+}$*Fgfr2*$^{flox/flox}$; hereafter, *Fgfr2*^{cnull})[24,25]. Analysis of E13.5 *Fgfr2*^{cnull} embryos revealed the absence of lungs but preserved the trachea and esophagus, as in the wild type (WT) (Fig. 1a), confirming the essential function of Fgfr2 selectively in lung formation[21,23]. The lack of placenta and limb defects in *Fgfr2*^{cnull} further suggested that the targeted gene-deletion strategy was well suited for the generation of hosts for lung CBC (Fig. 1b). In an initial attempt to complement the defective lung organ niche in *Fgfr2*^{cnull} mutants, we used donor PSCs derived from a *Nkx2–1-GFP* knock-in mouse[26]. These cells not only carry both Fgfr2 alleles but also express green fluorescent protein (GFP) from the NK2 homeobox 1 (*Nkx2–1*) locus, marking all lung epithelial progenitors and descendants from their earliest stages. Complemented PSCs$^{Nkx2-1-GFP}$ were expected to respond to Fgf10 from the host to form the lungs. PSCs$^{Nkx2-1-GFP}$ were cultured in medium containing selective GSK3β and Mek 1/2 inhibitors and Leukemia Inhibitory Factor (2i/LIF)[27], reported to maintain the ground-state pluripotency and the naive state of PSCs, and then were injected into Fgfr2-mutant host blastocysts and transferred to pseudopregnant mothers. The PSC$^{Nkx2-1-GFP}$ indeed outcompeted the host *Fgfr2*^{cnull} cells and carried on lung morphogenesis. GFP labeling was detected in nearly 100% of the epithelium overlapping with Nkx2–1, and differentiation markers of airways (Scgb1a1, acetylated α-tubulin) and alveolar (Sftpc, Pdpn) cell types (Extended Data Fig. 1). Although they did not have obvious abnormalities in lobation or branching morphogenesis, these lungs did not form the distal saccules for gas exchange and so remained immature, and pups died at birth (Extended Data Fig. 1b). Thus, 2i/LIF-treated PSC$^{Nkx2-1-GFP}$ in *Fgfr2*^{cnull} hosts were likely to be unable to establish the epithelial–mesenchymal cross-talks that are required for the proper maturation of the lung at late gestation.

Then, we systematically tested different culture conditions for optimal maintenance of PSC pluripotency. This included medium with valproic acid (VPA)—a histone deacetylase inhibitor that improves PSC derivation and chimera formation efficiency[28,29]—and alternative 2i (a2i) medium, in which Mek kinase inhibitor is replaced by a Src kinase inhibitor to enhance PSC germline competency and developmental potential[30,31]. The efficiency of these conditions was initially assessed on the basis of the expression of stage-specific embryonic antigen 1 (Ssea1) and platelet endothelial cell adhesion molecule (Pecam), known as pluripotency markers associated with high ability to form chimeras[32] (Table 1). Because it was unclear why donor PSCs$^{Nkx2-1\text{-}GFP}$ led to inappropriate lung development, we tested additional cell lines. This included commercially available PSCs$^{CAG–GFP}$, which expresses GFP under the cytomegalovirus (CMV) enhancer, chicken β-actin promoter. The 2i/LIF treatment of PSCs$^{CAG–GFP}$ resulted in the lowest Ssea1 mean fluorescent intensity (MFI) and the lowest proportion of Pecam^{+}Ssea1^{+} PSCs among all culture conditions, regardless of the PSC type (Extended Data Fig. 2 and Supplementary Fig. 1). However, treatment with LIF and VPA (VPA/LIF) yielded the highest Ssea1 MFI in both PSCs$^{CAG–GFP}$ and PSCs$^{Nkx2-1\text{-}GFP}$ (Extended Data Fig. 2b,c). Thus we injected VPA/LIF-treated PSC$^{CAG\text{-}GFP}$ into host *Fgfr2*-mutant blastocysts and analyzed the pups at birth (P0, postnatal day 0). Among the 24 pups obtained, only 1 died (non-complemented *Fgfr2*^{cnull}); all others remained alive and active until they were euthanized ~6 h after birth, consistent with rescued functional neonatal lungs. Indeed, the morphological analysis showed well-formed saccules with extensive GFP labeling of alveolar type 1 and 2, and secretory club, multiciliated and neuroendocrine cells in airways (Fig. 1c–e and Extended Figs. 3 and 4). By contrast, mesenchymal GFP labeling, including that in endothelial, vascular and airway smooth muscle cells, was variable and overall was similar in chimeric WT or complemented *Fgfr2*^{cnull} animals (Extended Data Fig. 5a–c and Supplementary Fig. 2). Notably, in PSCs$^{CAG–GFP}$*Fgfr2*^{cnull} animals, the frequency of GFP^{+} epithelial cells in the lung was significantly higher (~80%) than in the trachea (Extended Data Fig. 4c). Thus, the lung agenesis and preserved trachea in *Fgfr2*^{cnull} hosts provided different opportunities for complementation, even within the same organ. Quantitative analysis of GFP^{+} cells in other organs showed no consistent evidence of the high chimerism seen in the lung (Extended Data Fig. 5d–f). This underscores the significance of the vacant organ niche for CBC-mediated lung complementation. However, VPA/LIF-treated PSCs$^{CAG–GFP}$*Fgfr2*^{cnull} embryos displaying low GFP signals in the skin or other organs frequently had lung abnormalities, such as incomplete unilateral rescue (Extended Data Fig. 6 and Table 1). This suggested that donor PSCs were not reaching the host's lung niche efficiently.

VPA is known to improve chimera formation[28,29], so we tested its effect in each culture condition to identify the combination with the greatest capacity to induce pluripotency markers and sustain chimerism throughout development. We found that VPA and LIF (VPA/LIF) and a2i, VPA and LIF (a2i/VPA/LIF) treatments were equally efficient in generating the highest proportion of Ssea^{high}Pecam^{+} PSCs$^{CAG–GFP}$. However, the expression of the key pluripotent factor octamer-binding transcription factor 4 (Oct-4) was significantly higher in a2i/VPA/LIF cultures (Extended Data Fig. 7a,b). When injected into WT blastocysts, donor a2i/VPA/LIF-treated PSC$^{CAG–GFP}$ nearly maximized the chimera-forming ability in all tested conditions (Extended Data Fig. 7c,d and Table 1). This was further confirmed

using a population of a2i/VPA/LIF-treated Ssea1^{high} PSCs$^{CAG–GFP}$ isolated by fluorescence-activated cell sorting (FACS) (Ssea1^{high}, 71.4%; Ssea1^{dim}, 15.4%; Fig. 2a).

Injection of a2i/VPA/LIF-cultured Ssea1^{high} PSCs$^{CAG–GFP}$ into blastocysts from *Fgfr2*^{cnull} hosts consistently rescued the lung agenesis phenotype, regardless of host genetic background (Table 1). Of note, the CBC-rescued *Fgfr2*^{cnull} neonates were viable and active at birth, and were indistinguishable from their WT littermates. Flow cytometry analyses of the neonatal lungs from these animals showed that the proportion of GFP$^+$ cells was consistently higher in the lung epithelial cells (Epcam$^+$CD45$^-$Pecam$^-$: 94.8 ± 2.1%) than the variable GFP$^+$ contribution to the endothelium (Pecam$^+$CD45$^-$ Epcam$^-$: 62.0 ± 21.5%) and to other lung mesenchymal cells (the CD45$^-$Epcam$^-$Pecam$^-$: 64.3 ± 24.7%). Moreover, the proportion of GFP$^+$ cells in Epcam$^+$ epithelial cells from conditional heterozygous mutant *Fgfr2*^{hetero} (43.8 ± 12.4 %) and WT (45.5 ± 13.5%) complemented lungs was always variable and rarely reached the high values found in *Fgfr2*^{cnull} lungs (Extended Data Fig. 8a,b, Table 1 and Supplementary Table 1). It was indeed remarkable that the consistent (epithelial) versus variable (mesenchymal) complementation that resulted from emptying the host's epithelial niche was already evident, even in the relatively small number of *Fgfr2*^{cnull} pups compared with the other genotypes. FACS-based assessment of chimerism in the liver showed only a low proportion of donor GFP$^+$ cells, regardless of the host genotype (Extended Data Fig. 8c and Supplementary Table 1). Thus, a2i/VPA/LIF appeared to maintain PSC's pluripotency with high efficiency, which endowed high chimerism in the lungs and efficient complementation to rescue lung agenesis in *Fgfr2*^{cnull} neonates.

We had, however, no clear indication about why the PSCs cultured with a2i/VPA/LIF were more effective than the others. Given the key role of chromatin modifications and DNA methylation in PSC pluripotency and developmental potential[33], we investigated the epigenetic status of these PSCs to gain insights into the prospective mechanisms underlying these differences. Analysis of global DNA methylation showed significantly lower levels of 5-mC long interspersed nucleotide element 1 (Line-1) repeats in a2i/VPA/LIF-treated PSCs compared with those treated with LIF alone. This overall lower methylation status favoring pluripotency was similarly found in 2i/LIF-treated conditions, consistent with the global DNA hypomethylation reported in the naive state of mouse PSC pluripotency[33] (Extended Data Fig. 9a). Moreover, gene-expression analysis showed that a2i/LIF and 2i/LIF treatment of PSCs led to a trend toward a decrease in levels or significantly lower levels of the de novo DNA methyltransferase Dnmt3b, compared to LIF or VPA/LIF treatments, respectively. Interestingly, the differences in Dnmt3b expression in cells treated with a2i/LIF/VPA compared with other groups and the somewhat decreased but variable changes in expression of Dnmt3a (Extended Data Fig. 9b) and cofactor Dnmt3l (not shown) suggested the presence of additional players, such as the Dnmt-interacting proteins[34].

We next investigated potential differences in patterns of histone modifications. Western blot analyses showed that among all groups, a2i/VPA/LIF PSCs expressed the lowest levels of the repressive chromatin mark H3K27me3 (Extended Data Fig. 9c). Also, a2i/LIF-treated PSCs, regardless of VPA addition, were markedly enriched in H4 pan acetylation compared with 2i-treated PSCs. Immunofluorescence staining of H4 acetylation (Ace-H4) and quantitative analysis of relative MFI showed the strongest signals most consistently

in a2i/LIF (with or without VPA) compared to other conditions. Although some LIF-treated PSCs exhibited strong signals, overall, there was a broad range of intensities from very high to low, reflecting high variability and inconsistent effect (Extended Data Fig. 9d). Notably, activation marks other than Ace-H4, such as H3K4me or H3K27ac (Extended Data Fig. 9c and data not shown) were not enriched by a2i/LIF treatment. Therefore, the a2i/VPA/LIF cocktail generates a unique epigenetic state that includes DNA hypomethylation, low levels of H3K27 methylation and increased abundance of H4 acetylation. We propose that the combination of these epigenetic changes, resulting in a more accessible (open) chromatin, underlie the a2i/VPA/LIF-mediated enhanced expression of pluripotency-associated proteins, such as Oct4, Pecam and Ssea1. A more detailed analysis of these mechanisms is currently under investigation.

We then used our CBC approach to test whether a2i/VPA/LIF enhanced the developmental potential of Ssea1^{high} PSCs$^{CAG–GFP}$ to generate lungs fully functional throughout life. Two distinct mouse models of agenesis were used as hosts: the former *Fgfr2*^{cnull}, in which tracheal and lung progenitors are specified but the lung progenitors are selectively unable to expand, and the *Ctnnb1*^{cnull} (*Shh*$^{cre/+}$*Ctnnb1*$^{flox/flox}$), in which none of these progenitors are specified and thus neither lung nor trachea forms[19,20]. These enabled us to assess whether targeting different genes that are crucial for respiratory organogenesis under the same CBC strategy allowed these phenotypes to be rescued as expected. Remarkably, in both models, the chimeric animals with lung complementation developed normally to adulthood and reached full maturity (Figs. 2 and 3 and Extended Data Fig. 10). Pulmonary function tests (Flexivent) performed in adult mice showed values of airway resistance, lung elastance and compliance comparable with those of WT littermates. When challenged with a spasmogenic agent (methacholine), CBC-complemented lungs showed concentration-dependent bronchoconstriction indistinguishable from the response of controls (Figs. 2b,3c, Extended Data Fig. 10b and Table 1). Macroscopic analysis of *Ctnnb1*^{cnull}, PSC$^{CAG–GFP}$ mice showed strong GFP signals in both trachea and lungs, suggesting efficient donor complementation in all respiratory progenitors (Fig. 3a, Extended Data Fig. 10e). In *Fgfr2*^{cnull}, PSC$^{CAG–GFP}$ complementation occurred preferentially in the lung, compared to the trachea (Fig. 2c, Extended Data Fig. 4c and data not shown). Immunofluorescence of lungs from *Fgfr2*cnull, PSCCAG–GFP and *Ctnnb1*cnull, PSCCAG–GFP animals confirmed extensive GFP overlap with markers of the airway and alveolar epithelial cell types (Figs. 2c and 3a,b and Extended Data Fig. 10a,e).

In summary, we established a conditional gene-ablation strategy to vacate a specific niche for complementation (CBC) coupled with a new methodology for enhancing PSC chimerism and developmental potential, which uniquely maintains an open chromatin status and pluripotency in donor cells. The approach takes advantage of bona fide tissue interactions in vivo to overcome the substantial hurdles in generating lung and trachea in host embryos with a severe genetic defect that prevents these structures from forming. Complementation of defective respiratory progenitor niches resulted in the formation of fully functional lungs in vivo. The observations presented here open exciting perspectives for the use of CBC to generate epithelial and non-epithelial components of the lung employing tissue-specific Cre lines in hosts. Ongoing testing of various strategies of Cre-mediated recombination and our PSCs culture conditions suggest that CBC, coupled with efficient PSC maintenance,

is versatile and may be used to complement multiple layers to generate a functional lung wholly from donor cells. Our work also lays the conceptual and technical platforms for investigating mechanisms of cell competition during mammalian organogenesis or as part of the surveillance mechanisms that maintain tissue integrity in adult homeostasis and regeneration–repair. Challenges for future use of this technology in translational and clinical practice include the need for a better understanding of the mechanisms of immune tolerance and interspecific histocompatibility barriers to overcome tissue rejection, and strategies to ablate residual host cells selectively in the targeted organs preserving tissue integrity. Further progress in these areas will facilitate engineering complex organs, such as the lung in large animals, to be ultimately used in cell-based interventions for regenerative purposes in human diseases.

Methods

Mouse lines and genotyping.

Shh$^{Cre/+}$ mice (cat. no. 05622) and *Ctnnb1*$^{flox/flox}$ (Ctnnb1^{tm2Kem}: cat. no. 004152) were obtained from the Jackson Lab. For conditional deletion of Fgfr2 (*Fgfr2*^{cnull}) or Ctnnb1 (*Ctnnb1*^{cnull}), we crossed *Fgfr2*$^{flox/flox}$ or *Ctnnb1*flox/flox females with *Shh*Cre/+*Fgfr2*flox/+ or *Shh*Cre/+*Ctnnb1*flox/+ males, respectively. Genotyping of the *Shh*^{Cre} allele was performed by PCR according to the protocol provided by the vendor (Jackson Lab, cat no. 05622). *Fgfr2*$^{flox/flox}$ mice were kindly gifted by X. Zhang. We further backcrossed these mice for more than three generations with CD-1 mice (Charles River, strain code: 022). For the lung complementation analyses, we injected the following PSCs into blastocysts of *Fgfr2*^{cnull} or *Ctnnb1*^{cnull} and littermate controls (WT, *Fgfr2*^{hetero} or *Ctnnb1*^{hetero}): PSC$^{Nkx2-1-GFP}$ passage 15 (W4/129S6: a gift from L. Oikonomou and D. Kotton, CReM, Boston University), PSC$^{CAG–GFP}$ passage 10–11 (C57BL/6N × 129S6 background, MTI-GlobalStem: cat. no. GSC-5003). To assess the impact of PSC culture conditions we also injected the following PSC lines into WT blastocysts (Table 1): ES1$^{CAG–tdTomato}$ (C57BL/6N background), B7 (C57BL/6N background), SUN107.4 (CD1 background) derived at Stanford University; CSL2J2 (C57BL/6J C2J background), FL19 ARR3–1 (albino agouti C57BL/6N background), FL19 ARR3–2 (C57BL/6N background) derived at the Columbia University Transgenic Core Facility. Genotyping of Fgfr2 + PSC$^{CAG–GFP}$ or Ctnnb1 + PSC$^{CAG–GFP}$ chimeric animals was confirmed by GFP-negative sorted liver cells or a single-cell colony formation assay of hematopoietic progenitor cells prepared with an EZ Fast Blood/Cell PCR Genotyping Kit (EZ BioResearch cat. no. G1002). Briefly, we performed PCR using the following Tm-adjusted primers, which allowed us to obtain equal band size in heterozygous *Fgfr2* allele: FR2-F1, 5′-ATAGGAGCAACAGGCGG-3′, and FR2-F2, 5′-CAAGAGGCGACCAGTCA-3′ resulting in a 142 base pair (bp) product for the WT allele and a 207 bp product for the conditional, *Fgfr2* floxed, allele 5′-AAG GTA GAG TGA TGA AAG TTG TT-3′, and 5′-CAC CAT GTC CTC TGT CTA TTC-3′ primers were used to detect the *Ctnnb1*-mutant allele (~300 bp) and wild-type allele (223 bp)[35]. A separate set of primers, FR2-F1 and FR2-F3, 5′-CATAGCACAGGCCAGGT-3′ were used to detect the *Fgfr2* locus following recombination by Cre recombinase (244-bp product)[25]. For PSC$^{Nkx2-1-GFP}$ mice, we performed PCR for the detection of a *Shh*^{Cre} allele in the tail tissue samples and further confirmed the Fgfr2 expression in the GFP-negative tracheal

epithelial layers using Fgfr2-specific antibody (Santa Cruz, sc-6930). The antibody signal was amplified by the Tyramide Signal Amplification kit (Perkin Elmer, NEL704A001KT, TSA-Cy3 1:100 dilution). The GFP fluorophore in P0 pup skin was activated by Dark Reader Handlamp (Clare Chemical Research, HL34T) and monitored by digital camera video mode through the Reader viewing filters (Clare Chemical Research, AG16).

Immunofluorescence.

Tissue sections or cultured PSCs were incubated with primary antibodies overnight at 4 °C, washed in PBS and incubated with secondary antibody conjugated with Alexa488, 567 or 647 (1:300) with NucBlue Fixed Cell ReadyProbes Reagent (DAPI) (Life tech., Ra37606) for 1.5 h. Samples were washed with PBS and mounted with ProLong Gold antifade reagent (Invitrogen, P36962). IF analysis was performed in 10-μm sections from WT, *Fgfr2*$^{\text{hetero}}$ or chimeric mice at P0 or P80 using the M.O.M. (mouse on mouse) kit (Vector Laboratories) according to the manufacturer's protocol. Antigen retrieval was performed using Unmasking Solution (Vector Laboratories H-3300) and microwaving of samples for 3 min at around 100 °C. The following antibodies were used: anti-acetylated β-tubulin IV (Abcam, ab11315, 1:500), anti-GFP chicken polyclonal antibody (pAb) (Thermo Scientific, 1:500), anti-Scgb1a1 goat (Santa Cruz, sc-9772, 1:500), anti-Pdpn (R&D, AF3244, 1:200), anti-Hop (Santa Cruz sc- 398703, 1:100), anti-Sftpc (Seven Hills WRAB-9337, 1:1,000), anti-Cgrp (Sigma, C8198, 1:1,000), anti-Sox2 rat (eBiosience, 14–9811-82), anti-SMA rabbit (Cell Signaling, 19245), anti-Oct4 (Gentetex, GT486, 1:100), anti-SSEA1 (SantaCruz, sc-101462, 1:50), anti-Oct4 (R&D, AF1759) and Histone H4ac (pan-acetyl) (Active Motif, 39925). Isolectin B4 (Life Tech., I32450) was used at a dilution of 1:500 in PBS overnight at 4 °C prior to the staining above to visualize vascular endothelial cells. For the whole-mount staining, we used SeeDB2 methods[36]. Images were acquired using a Nikon Labophot 2 microscope equipped with a Nikon Digital Sight DS-Ri1 charge-coupled device camera or on a Zeiss LSM710 confocal laser scanning microscope or using 3D-SIM microscopy[37].

Preparation of pluripotent stem cells.

We cultured PSC$^{Nkx2-1\text{-}GFP}$ cells (passage 15) for 5 days before blastocyst injection with 2i/LIF medium[31] containing 1 μM PD0325901 (Tocris, no. 4192), 3 μM CHIR99021 (Tocris, no. 4423) and LIF (1000 U ml^{-1}, Millipore, no. ESG1106) in DMEM based-serum medium (Gibco no. 11995, cat. no. 10569–044) supplemented with 14% ESC qualified FBS (Hyclone SH30070.03E), Glutamax (Giboco, no. 35050061), NEAA (Invitrogen, no. 11140050), 0.1 mM BME (Sigma, no. M6250) and pen/strep (Gibco, no. 30-001-CI). To assess the impact of each defined PSC medium on the maintenance of PSCs (PSC$^{Nkx2-1\text{-}GFP}$, PSC$^{\text{CAG–GFP}}$), these were cultured for 5 days on irradiated MEFs (CF1 mouse embryonic fibroblasts, Life tech, no. A34181) in DMEM-based serum medium containing LIF (2000 U ml^{-1}) for LIF, further supplemented with 0.5 mM VPA (Sigma, no. P4543) for VPA/LIF; 1.5 μM CGP77675 (Sigma no. SML0314) and 3 μM CHIR99021 for a2i/LIF; 1 μM PD0325901 and 3 μM CHIR99021 for 2i/LIF; 1 μM PD0325901 and 3 μM CHIR99021, 0.5 mM VPA (Sigma, no. P4543) for 2i/VPA/LIF; and 3 μM CHIR99021, 1.5 uM CGP77675 (Sigma no. SML0314), 0.5 mM VPA (Sigma, no. P4543) for a2i/VPA/LIF, respectively[29,31]. MEFs were prepared at a density of 2 × 10^6 per a six-well plate in DMEM-based MEF medium the day before plating PSCs[38]. These PSC cells were

passaged at a split ratio of 1:6 every 2–3 d. For the analyses of flow cytometry, we used $PSC^{CAG–GFP}$ cultured for 5 days in each experimental condition. Briefly, cultured cells were trypsinized for 30 s–1 min with 0.05% trypsin, and were resuspended in 10 ml cold DMEM + 10% FBS, immediately. Samples were centrifuged for 3 min at room temperature at 1,000 r.p.m., and the supernatant was removed. After filtering the cells with a 35-μm nylon mesh (FisherScientific, 08–771-23), we performed live-cell staining on ice for 20 min with the following antibodies and dyes in cold flow buffer (PBS + 0.2% BSA) according to the manufacturer's protocol: SSEA1-BV421 (BioLegend, 125613: 1:200 dilution), PECAM-APC (BioLegend, 102509: 1:200 dilution), Zombie Aqua Fixable Viability Kit (BioLegend, 423101). We performed flow cytometry by BD LSR II Flow Cytometer and performed analysis using FlowJo software (Fig. 2a and Extended Data Fig. 2b,c). Statistical analyses were performed using a one-way analysis of variance (ANOVA) for the evaluation of the proportion of $Ssea1^{+}Pecam^{+}$ $PSCs^{Nkx2-1-GFP}$ among the parental population (live cells) in three independent biological samples per each condition. For immunofluorescence analyses of Oct4 and Ssea1 expression, we fixed the cells with 4% PFA for 15 min at room temperature and stained with each antibody, as described above.

Quantification of the pluripotency markers in the colonies of pluripotent stem cells.

Images of Oct4, Ssea1 or pan-acetyl Histone H4 staining were captured using the same parameters for each cell culture condition using a DMi8 (Leica Microsystems) inverted microscope. We performed quantitative analyses using ImageJ software. Briefly, we acquired Oct4- or pan-acetyl Histone H4 MFI of each colony cultured in the six different conditions (LIF, 2i/LIF, a2i/LIF, VPA/LIF, 2i/VPA/LIF, a2i/VPA/LIF) on the basis of the histogram of ImageJ program (Analyze > Histogram). The edge of each colony was manually selected using a freehand selection tool of ImageJ. Twenty colonies from five different fields of each cell-culture condition were randomly selected for Oct4 and Ssea1 co-staining or pan-acetyl Histone H4 staining per experiment. To acquire relative MFI, we subtracted the background MFI of randomly selected non-colony area from 5 different fields, and then each subtracted MFI was normalized by dividing the average of MFI of the 20 colonies in LIF condition. The graphs are representative of three independent experiments. Then, we performed a Student's *t*-test for the statistical analyses of Oct4 and Ssea1 co-staining or pan-acetyl Histone H4 staining for the tested conditions. For the quantification of single Ssea1 staining by immunofluorescence, 5 random fields containing 11.5 colonies per field were captured using a DMi8 Leica microscope. Then, we classified those colonies into three categories based on the signal intensity of SSEA1 ($Ssea1^{high}$, $Ssea1^{dim}$, or $Ssea1^{-}$ (representative images in the upper panels of Extended Data Fig. 7a). We generated the graphs to represent means and standard errors ($n = 5$ fields) depicting the proportion of those categories in each condition. Each graph of Ssea1 analyses was representative of three independent experiments. Results from $Ssea1^{high}$ PSC in each condition were subjected to statistical analyses (one-way ANOVA), expressed as mean + s.e.m., and differences were considered statistically significant at $P < 0.05$).

Analysis of GFP^{+} chimerism by flow cytometry.

To obtain the percentage of GFP^{+} cells in lung endothelial, mesenchymal and epithelial cells simultaneously in the littermate chimeric mice of *Fgfr2*cnull; *Rosa*tdTomato/+,

*Fgfr2*hetero; *Rosa*tdTomato/+ or WT, we used the protocol previously reported[39,40] with minor modification for the P1 respiratory tissue analyses. Briefly, we harvested the lungs and tracheas from those chimeric mice at P1 and placed the tissues into 50-ml tubes containing 10 ml of cold Ham's F12 medium. After transferring the tissues into 1.5-ml Eppendorf tubes, we finely minced the tissues by scissors. We then added 100 µl of pre-warmed dissociation buffer (1 mg ml^{-1} DNase (Sigma), 5 mg ml^{-1} collagen (Worthington Biochemical Corporation) and 15 U ml^{-1} Dispase (Corning) in HBSS). We then minced the tissues again to make them smaller than 3 mm in size. We then added 900 µl of pre-warmed dissociation buffer (total 1 ml dissociation buffer), and incubated them at 37 °C on the rocker with 135 r.p.m. speed. After 30–45 min of the incubation, we put the tubes back on the ice and filtered the digested tissues by the 40-µm filter (FALCON cat. no. 352235). The filtered tissues were centrifuged at 1,400 r.p.m., 4 °C, for 5 min, and we removed its supernatant. We resuspended the cell pellets with 1.5 ml of cold ACK lysis buffer to lyse remaining erythrocytes for 3 min at RT. We added 3 ml cold HBSS and centrifuged them down at 1,400 r.p.m., 4 °C, for 3 min to remove the lysed blood cells. Then, we resuspended the cell pellets with 1 ml cold HBSS + 0.2% BSA and counted the cell number (about 3 million per P1 lung) with a hematocytometer. We transferred 1–1.5 million cells in 500 µl (final volume) of flow buffer (cold HBSS, 0.2% BSA and 5 uM Y27632), and then added 10 µl Fc Block (BD Pharmingen; cat. no. 553141) per sample and incubate for 10 min at 4 °C. Then, we added the following antibodies: PECAM-BV421 (BD Pharmingen, cat. no. 562939, 1/250 dilution), EPCAM-BV711 (BioLegend, 118233, 1/200), Aqua Zombie (BioLegend, 423101, 1/500), CD45-BV605 (BioLegend, 103155, 1/200) for 30 min on ice. After the staining, we washed the samples with flow buffer and resuspended them in 500 µl flow buffer for the subsequent analyses by Flow cytometer (FACS Aria; gating strategy in Extended Data Fig. 8). For setting up compensation and the voltage of each channel to avoid the background of autofluorescence and spill over each fluorophore signal to the other channels, we acquired 5×10^5 events from unstained control sample (WT CD1 mouse P1 lungs and trachea), each single staining sample (WT CD1 mice P1 lungs and trachea), $PSC^{CAG–GFP}$ (for GFP^+ events) and $ES1^{tdtomato}$ (for $tdTomato^+$ events). For Zombie Aqua staining, we used WT CD1 mice P1 lungs and trachea incubated on ice to increase the population of dead cells (shown in Extended Data Fig. 8).

Blastocyst preparation and embryo transfer.

Blastocysts were prepared by mating *Shh*^{Cre}; *Fgfr2*$^{flox/+}$ males with superovulated *Fgfr2*$^{flox/flox}$ females. For testing the effect of different culture conditions, we used WT (C57BL/6N × 129S6x CD1) males and females. Briefly, PMSG (pregnant mare serum gonadotropin, 5 IU in 0.1 ml PBS per mouse) was administered 48 h prior to mating, and hCG (5IU in 0.1 ml PBS per mouse) was administered 12 h before its mating as an intraperitoneal injection[15]. Blastocysts were harvested at E2.25, and 8–20 PSCs were injected into each blastocyst (Table 1). After the PSC injection, blastocysts were cultured in M2 medium (Cosmobio) for a few hours in a 37 °C, 5% CO_2 incubator for its recovery. Then, blastocysts were transferred to the uterus of the pseudopregnant foster mother, according to a protocol approved by the Columbia University Institutional Animal Care and Use Committee.

Sorting liver cells for genotyping.

Genotyping of the chimeric mice was performed in liver cells prior to fixation for histological analyses. Briefly, the dissected liver tissue from each pup (P0, P1) or embryos (E12.5, E15.5) was sliced (0.5 cm × 0.2 cm) and minced for 5 min using scissors. Tissues were trypsinized with 500 μl 0.25% trypsin (Invitrogen) for 15 min at 37 °C, and the enzyme was inactivated with an equal amount of cold 100% fetal bovine serum (FBS). These cells were centrifuged at 1,000 r.p.m., 4 °C, 5 min, and the supernatant was removed. Cells were resuspended in 1 ml flow buffer (PBS + 0. 2% bovine serum albumin (BSA), passed through a 40-μm-pore nylon-mesh filter and transferred into a flow tube. Cells were stained with DAPI (1/1,000) for 5 min to remove dead cells. More than 10,000 cells per liver were sorted by FACS Area with the GFP-negative gate used for genotyping. The sorting purity was usually more than 90%. After removing the flow buffer by centrifuging at 1,000 r.p.m., 4 °C, 5 min, cells were then stored at −20 °C. We performed PCR with Tm-adjusted primers and the GFP-negative population as a template. The chimerism (measured as % GFP^+/live cells) in the liver cells was analyzed from the fcs files of sorted data by FlowJo.

Hematopoietic progenitor cells in colony-forming unit assays for genotyping of adult chimeric mice.

To determine the genotyping before the pulmonary function test in the live chimeric adult mice, we performed a colony-formation assay in the MethoCult medium (Stemcells, no. M3434). Briefly, we harvested 0.2 ml into the 1-ml Eppendorf tube containing 20 μl 0.5 mM EDTA blood from the submandibular vein of chimeric mice by using a 5 mm lancet[41]. After the treatment with RBC lysis buffer (BioLegend, no. 420301) to each blood sample according to the manufacture's protocol, we removed lysed blood cells contained in the supernatant and, kept cell pellets it in 100 μl cold PBS. After counting these cell numbers, we plated each 0.4×10^5 cells per well resuspended in 300 μl MethoCult medium containing 100 μg ml^{-1} Primocine (IvivoGen, no. ant-pm-1) in a 24-well plate. Since the MethoCult medium is highly viscous, we used blunt-end needles, 16 gauge (Stemcells, no. 28110) to plate the cells equally in 24-well plates. We could obtain about 10 isolated colonies per 3 wells, and then we manually picked up at least 5 colonies from each mouse blood sample by using a 10-μl pipette for the subsequent genotyping analyses by using EZ Fast Blood/Cell PCR Genotyping Kit (EZ BioResearch cat. no. G1002).

Morphometric analyses.

To determine the relative number of specific cell populations in P0 chimeric lungs, 10 non-overlapping random fields per mice were analyzed (×20 magnification) after capturing the images by confocal microscopy (Zeiss LSM710)[42]. For each field, we counted the number of GFP^+ cells co-immunostained with specific antibodies. DAPI co-staining was used to determine the cell number for each lineage as identified by differentiation markers, such as Sftpc, β4-tubulin and CC10, for alveolar type 2 cells, multiciliated cells and club secretory cells, respectively. Sox2 was used as a general marker for airway epithelial cell progenitors. Statistical analysis was performed (Student's *t*-test) and differences were considered significant if $P < 0.01$. $Pdpn^+GFP^+$ area, $Pdpn^+Hopx^+GFP^+$ triple-positive area for the type 1 cells and $PECAM^+GFP^+$ area for vascular endothelial cells were calculated

by Image J (NIH). Briefly, 10 non-overlapping random fields per mouse were captured using the same confocal microscopy settings. Each signal threshold of GFP, Pdpn, Hopx and Pecam was determined on the basis of each negative control: non-chimeric mouse tissue section of *Shh*^{Cre}; *Fgfr2*$^{flox/+}$ against GFP signal; secondary antibody only against each signal of Pdpn, Hopx and PECAM. The Hopx^{+}Pdpn^{+} double-positive area was determined by pasting Hopx stained image on the corresponding field of the Pdpn-stained image, and the non-overlapped area was subtracted by ImageJ. The percentage of GFP labeling is determined by the following formula: Pdpn^{+}GFP^{+}/Pdpn^{+} × 1.453 (normalization value) × 100, Pdpn^{+}Hopx^{+}GFP^{+}/Pdpn^{+}Hopx^{+} × 1.406 (normalization value) × 100, Pecam^{+}GFP^{+}/PECAM^{+} × 1.306 (normalization value) × 100. Each normalization value was determined based on the average ratio of five overlapping fields of *Fgfr2*^{cnull} + GFP samples. For example, in the case of Pdpn, the normalization value was (Pdpn^{+} area)/(Pdpn^{+}GFP^{+} area) in the five Pdpn^{+}GFP^{+} overlapping fields of *Fgfr2*^{cnull} + GFP samples.

Quantitative real-time PCR.

We treated the cells for 5 days in 6 different cell-culture conditions (LIF, LIF/2i, LIF/a2i, VAP/LIF, 2i/VPA/LIF and a2i/VPA/LIF). Total RNA from each cell sample was extracted using the RNeasy Mini Kit (Qiagen, no. 74104) and reverse-transcribed using Superscript III (Invitrogen, no. 18080–051). Reactions (25 μl) were performed using ABI 7000 (Applied Biosystems) and SYBR Green Master Mix (Thermo Fisher, no. A25741). The relative abundance of the RNA for each gene to β-actin mRNA was determined using the $2^{-\Delta\Delta Ct}$ method. The following primers were used: Dnmt3a forward 5′-CCTGCAATGACCTCTCCATT-3′; Dnmt3a reverse 5′-CAGGAGGCGGTAGAACTCAA-3′; Dnmt3b forward 5′-TGGTGATTGGTGGAAGCC-3′; Dnmt3b reverse 5′-AATGGACGGTTGTCGCC-3′. Data were represented as mean ± s.e.m. of measurements in each culture condition and analyzed by Student's *t*-test. Differences were considered statistically significant if $P < 0.05$; the number of animals per group are provided in the legends

Western blot analysis.

PSCs were cultured for 5 days (LIF, LIF/2i, LIF/a2i, VAP/LIF, 2i/VPA/LIF and a2i/VPA/LIF) and Western blot analysis was performed as reported previously[43]. Cells were lysed in laemmli buffer (Sigma, no. S3401) and boiled for 15 min at 95 °C. Lysates were then separated by SDS–polyacrylamide gel electrophoresis (SDS–PAGE), transferred to a nitrocellulose membrane, blocked in 5% nonfat milk in PBS plus 0.5% Tween-20, probed with primary antibodies, and detected with horseradish-peroxidase-conjugated anti-rabbit or anti-mouse secondary antibodies (GE Healthcare). The following primary antibodies were used: anti-Histone H4ac (pan-acetyl) (Active Motif, no. 39925, dilution 1:1,000), Histone H3K27me3 antibody (monoclonal antibody) (Cell Signaling Tech, no. 2901, dilution 1:1,000) and Histone H3K4me3 antibody (pAb) (Active Motif, no. 39915, dilution 1:1,000). Anti-Histone H3 (Abcam, no. ab1791, dilution 1:1,000) antibodies were used as internal controls. Enhanced chemiluminescence was detected using LAS 4000 (GE Health Care). Quantitative analysis for the western blots was performed by calculating the relative density of the immunoreactive bands after the acquisition of the blot image with a LAS 4000 CCD video camera module and analyzing with the Image 152 g program (Wayne Rasband, NIH,

Research Service Branch, NIMH, Bethesda, MD). Briefly, we subtracted the background density value (the average of five randomly selected equal size of the area) to the acquired density value of each blot. Then, we divided each subtracted density value by the subtracted value of the LIF sample for obtaining normalized relative values.

LINE-1 ELISA analyses.

To measure 5-mC levels of Long Interspersed Nucleotide Element 1 (LINE-1) repeats, we treated the cells for 5 days in 6 different cell culture conditions (LIF, LIF/2i, LIF/a2i, VAP/LIF, 2i/VPA/LIF and a2i/VPA/LIF). We performed ELISA-based LINE-1 analyses according to the manufactured protocol (Active Motif, no. 55017). Briefly, genomic DNA was enzymatically digested with MseI enzyme to generate the appropriate fragments to hybridize to a biotinylated consensus sequence. Hybridized samples were immobilized to a 96-well plate, and methylated cytosines are identified using a 5-methylcytosine antibody, HRP-conjugated secondary antibody and colorimetric detection reagents. Generating a standard curve using the included DNA standards with known LINE-1 methylation levels provided the relative level of 5-methylcytosine in each DNA sample. Statistical analyses were performed using one-way ANOVA. Results were expressed as mean + s.e.m., and differences are considered statistically significant if $P < 0.05$.

3D structured illumination microscopy.

To further demonstrate chimerism and complementation of alveolar type 1 cells (GFP and IF with Pdpn) at high resolution we used structured illumination microscopy (SIM), performed with a Nikon N-SIM based on an Eclipse Ti inverted microscope using an SR Apo-TIRF ×100/1.49 oil-immersion objective and an Andor iXon 3 EMCCD camera, as described previously[37]. Briefly, the images for each lung cell were acquired in 3D-SIM mode using excitation at 405 nm, 488 nm and 561 nm and standard filter sets for blue, green and red emission. Image *z*-stacks were collected with a *z* interval of 200 nm. SIM image reconstruction, channel alignment and 3D reconstruction were performed using NIS-Elements AR software. The images were visualized using an alpha-rendering mode that can show the signal of the structural surface.

Pulmonary function assessment.

Chimeric mutant mice (*Fgfr2*^{cnull} + PSC$^{CAG–GFP}$ or *Ctnnb1*^{cnull} + PSC$^{CAG–GFP}$) and its littermate control WT mice were anesthetized with pentobarbital (intraperitoneally, 50 mg per kg (body weight)). Once surgical anesthesia was achieved, mice were tracheotomized with an 18G cannula and connected to a flexiVent (SciReq, Montreal, Quebec, Canada) with an FX1.

Module and an in-line nebulizer were described previously[44]. Mice were mechanically ventilated at 150 breaths per min, with a tidal volume of 10 ml per kg and a positive end-expiratory pressure of 3 cm H_2O. Muscle paralysis was achieved with succinylcholine (i.p., 10 mg per kg (body weight)) to prevent respiratory effort. By using the forced oscillation technique, baseline measurements of the resistance (Rrs), compliance (Crs) and elastance (Ers) of the respiratory system were measured. A baseline measure of central airway resistance (Rn) was performed, followed by subsequent Rn measurements during

nebulized methacholine (0, 6.25, 12.5, 25 and 50 mg ml^{-1}) challenge (10-s nebulization, 50% duty cycle). Values for all measurements represent an average of three replicates. EKG and temperature were continuously monitored. Statistical analysis was performed by Student's *t*-test, paired. Results were expressed as mean + s.e.m. and differences considered statistically significant if $P < 0.05$. The number of animals per group are provided in the legends.

Study approval.

All experiments involving animals were performed according to the protocol approved by the Columbia University Institutional Animal Care and Use Committee and USAMRMC Animal Care and Use Review Office (ACURO).

Reporting Summary.

Further information on research design is available in the Nature Research Reporting Summary linked to this article.

Data availability

All files and processed data are also available from the corresponding author upon request. No database was generated. Source Data for Figs. 1–3 and Extended Data Figs. 2, 4, 5 and 7–10 are available online.

Extended Data

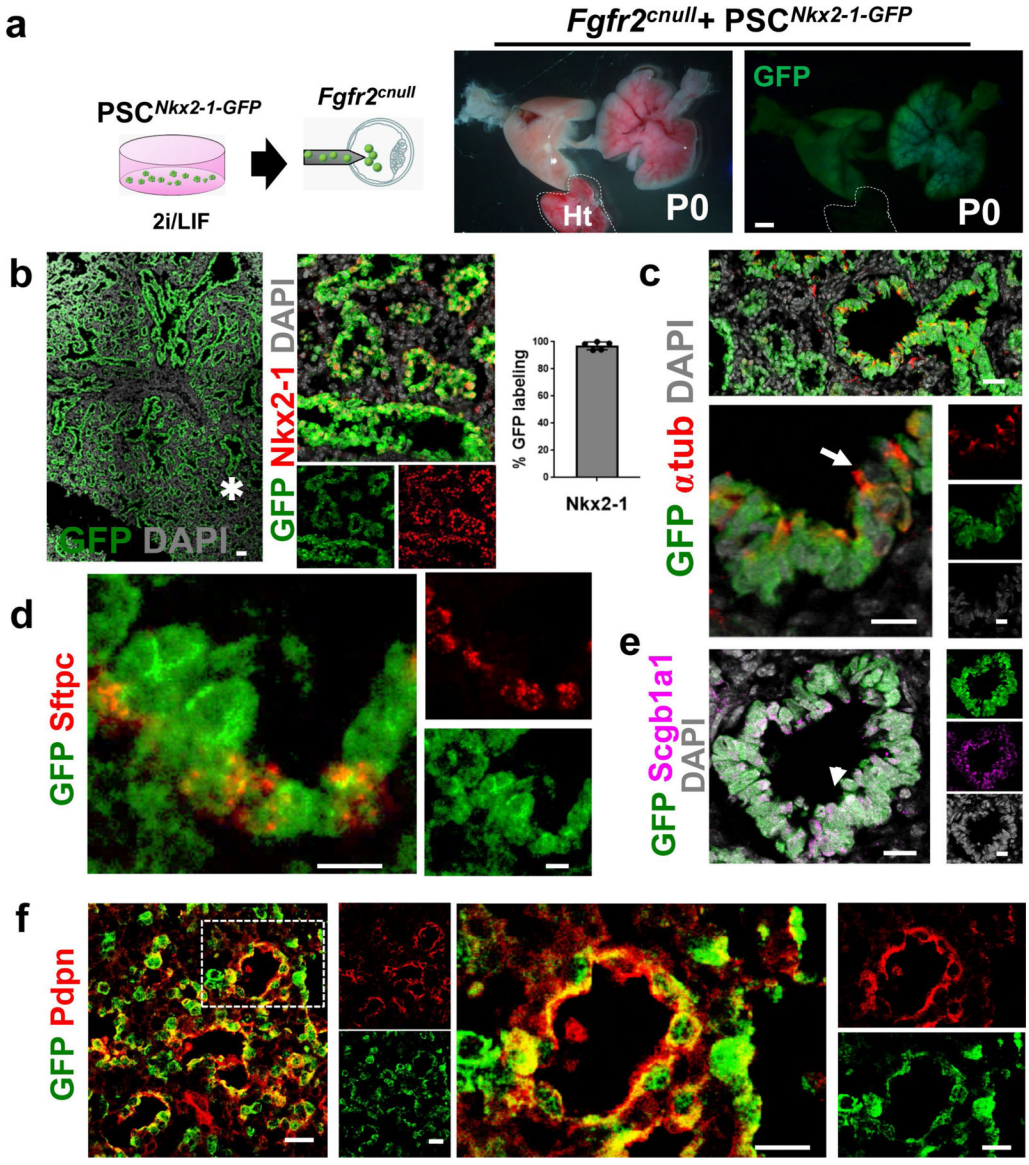

Extended Data Fig. 1 |. PSC$^{Nkx2-1-GFP}$ rescues lung agenesis in *Fgfr2*-deficient mutants, but lungs are immature.

a, Schematic of experimental procedure (left) and representative macroscopic view of the lungs and heart (ht) from newborn (P0) mice *Fgfr2*^{cnull} complemented by donor 2i/LIF-cultured *PSC*$^{Nkx2-1-GFP}$. Right panel depicts GFP signals in the lungs not present in the heart (outlined). **b**, Representative GFP expression in lung section of P0 *Fgfr2*^{cnull} + PSC$^{Nkx2-1-GFP}$: strong signals throughout all epithelial tubes, less prominent in the mesenchyme and its derivatives (Ex. large vessels, center). Asterisk (*) marks distal epithelial tubules unable to form distal saccules resulting in immature non-functional lungs. Immunofluorescence of Nkx2–1 and quantitative analysis confirming extensive double-labeling with GFP (single channels shown in small panels). Graph represents mean ± s.e.m. of % GFP+ lung epithelial cells in five random fields per sample (n = 2 animals). **c**–**f**,

Representative immunofluorescence and confocal images of lungs double-labeled with GFP and markers of alveolar type 1 (Pdpn) and type 2 (Sftpc) or airway multiciliated (acetylated α-tub) or secretory (Scgb1a1) cells (n = 3–4 per group). Boxed area (**f**) enlarged in the right panels. **b**–**f**, images also displayed as single channels; DAPI in grey. Scale bars: **a**, **b**, **c**–**e**, **f**: 1 mm, 20 μm, 10 μm, and 20 μm, respectively.

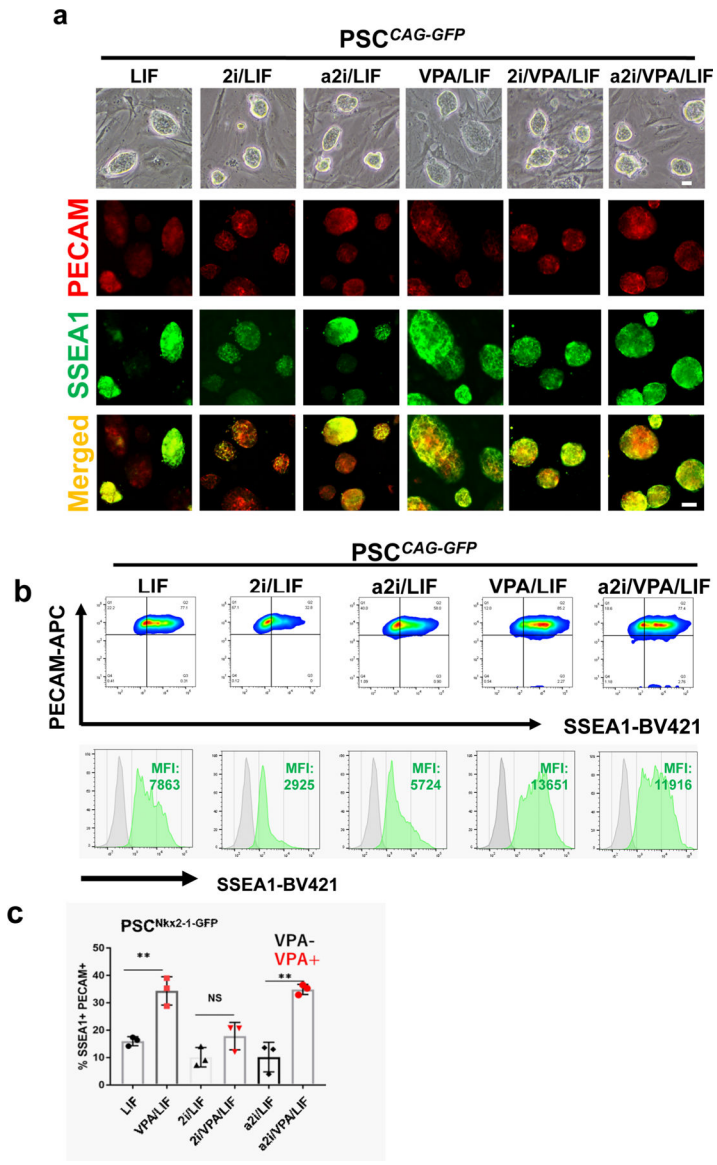

Extended Data Fig. 2 |. Effect of PSC cell culture conditions in pluripotency markers.
a, Representative morphology of PSC$^{CAG–GFP}$ colonies and immunofluorescence image of Ssea1 and Pecam expression under the culture conditions listed. **b**, Representative flow cytometry pseudocolor images (top) and respective histograms (bottom) showing the increased yield of the Ssea1^{high}Pecam+ PSC$^{CAG–GFP}$ population and high Ssea1 MFI in cultures treated with VPA/LIF and a2i/VPA/LIF. **c**, FACS analysis of PSC$^{Nkx2-1-GFP}$ cultured on the conditions indicated. Graph shows differences in the yield of Ssea1+Pecam+

(%). Note the effect of the addition of VPA to LIF or a2i/LIF treatment. Bars are mean ± standard error of $n = 3$ independent experiments in each culture condition. Data were analyzed by one-way ANOVA; differences were significant at $^{**}P < 0.01$. Scale bars: **a** = 10 μm.

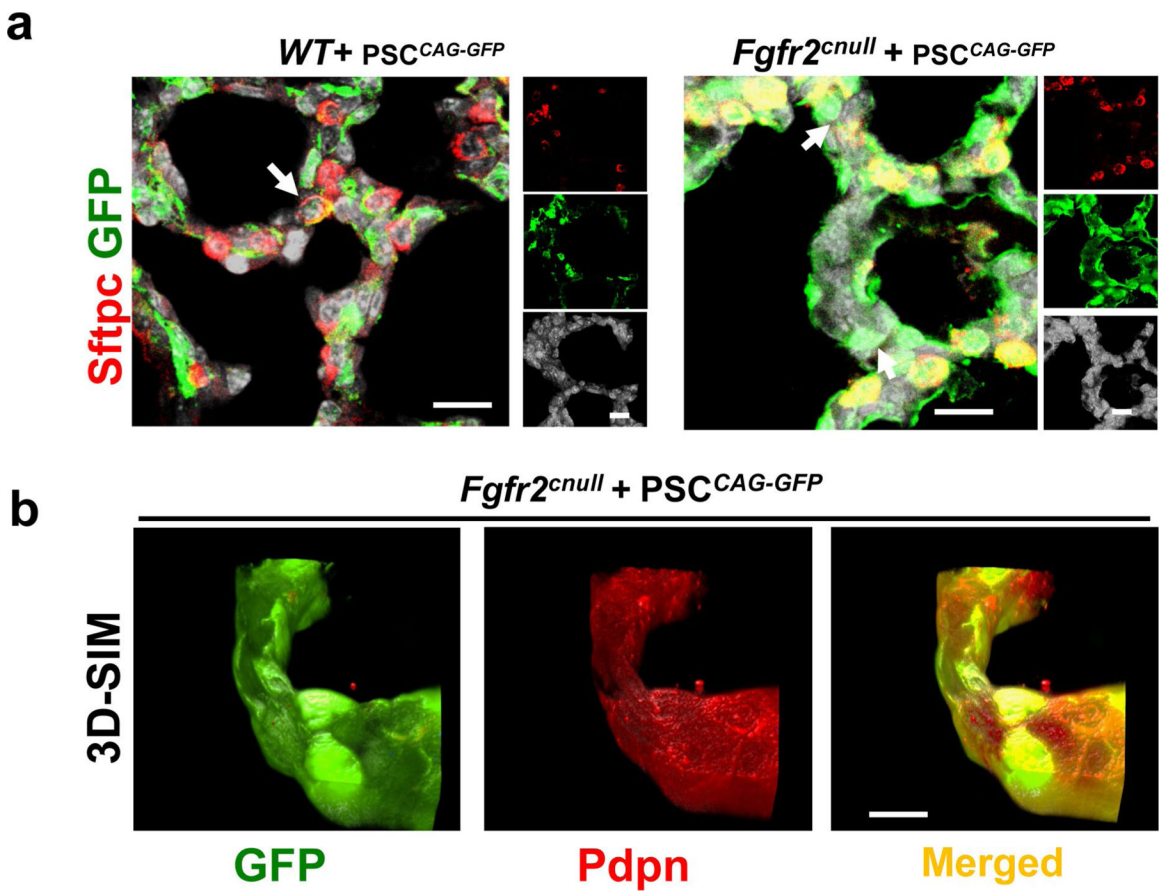

Extended Data Fig. 3 |. Complemented distal lung of VPA/LiF-treated PSC$^{CAG–GFP}$ *Fgfr2* mutants undergo sacculation.

a Representative immunofluorescence confocal imaging depicting the expression of GFP and markers for alveolar type 2 (Sftpc) in the walls of distal saccules in lung sections of P0 VPA/LIF-treated PSC$^{CAG–GFP}$ *Fgfr2*^{cnull} mice (left panel, WT P0 littermate). **b**, the 3D-SIM image of PSC$^{CAG-GFP}$ *Fgfr2*^{cnull} mice showing at high resolution the staining of alveolar type I surface double-labeled with GFP. Scale bars: **a** and **b**,10 μm.

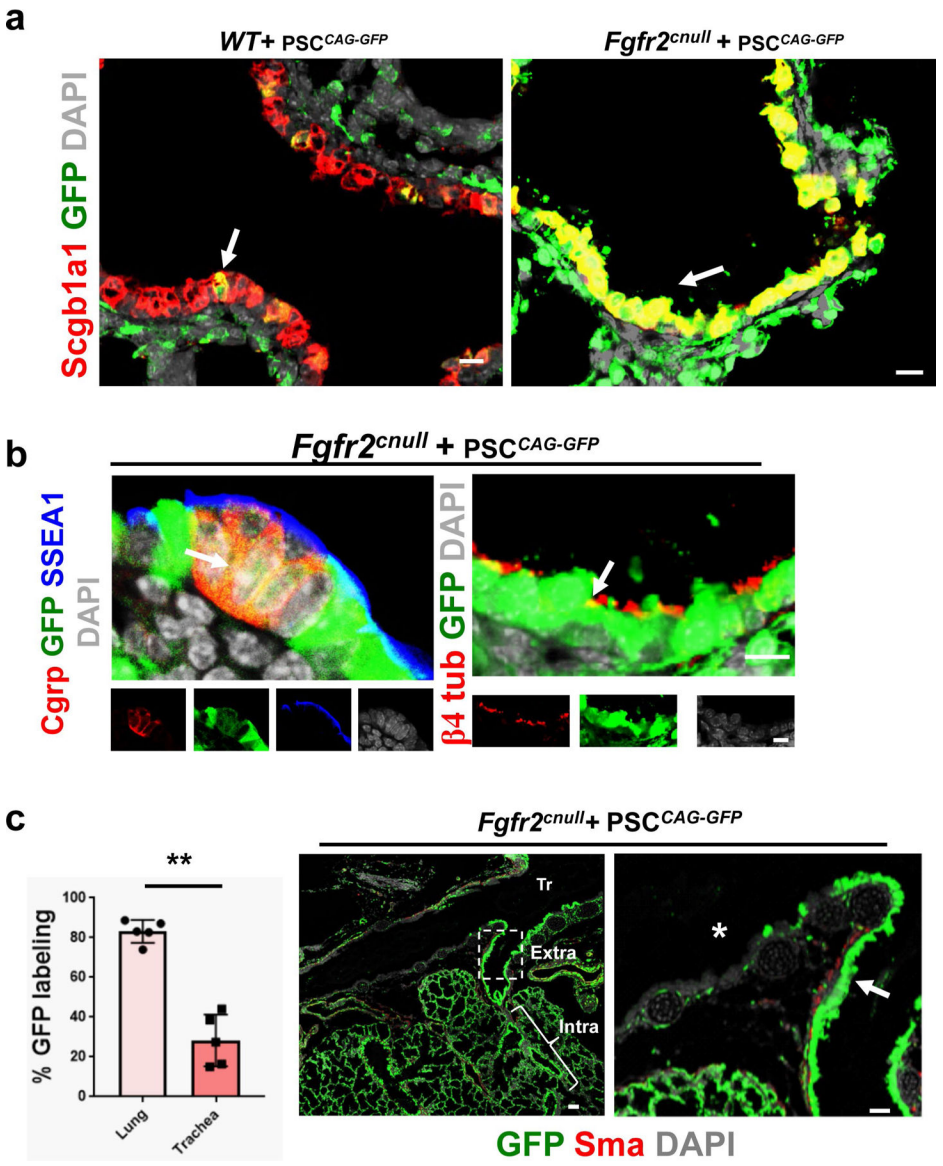

Extended Data Fig. 4 |. Airway epithelial complementation in *Fgfr2*^{cnull} PSC$^{CAG–GFP}$newborn chimeric pups.

a,**b**, Immunofluorescence and confocal imaging depicting GFP double-labeling (arrows) with cell differentiation markers Scgb1a1 (secretory), β-tubulin4 (multiciliated) and Cgrp (neuroendocrine) in lung sections of P0 mice from VPA/LIF-treated PSC$^{CAG–GFP}$ + *Fgfr2*^{cnull} and WT chimeric littermates; small panels in **b** depict single channels). **c**, Percentage of GFP+ cells in the lung and tracheal epithelium as determined by quantitative analysis of GFP signals in sections of newborn P0 PSC$^{CAG–GFP}$ *Fgfr2*^{cnull} animals. Graph, Mean ± s.e.m. of measurements in 5 random fields per section per sample. Student's *t*-test; $^{**}P < 0.01$. Right panel, Representative GFP and Sma immunostaining in a histological section of P0 complemented mutant depicting epithelial signals (arrows) consistently strong in intrapulmonary airways (bracket), but variable or low (asterisks) in the extrapulmonary airway (dashed box) and trachea (Tr). Boxed area enlarged on the right. Sma (alpha-smooth

muscle actin) labeling airway smooth muscle. Scale bars: **a**, **b**, **c**: 10 μm, 10 μm, and 20 μm, respectively.

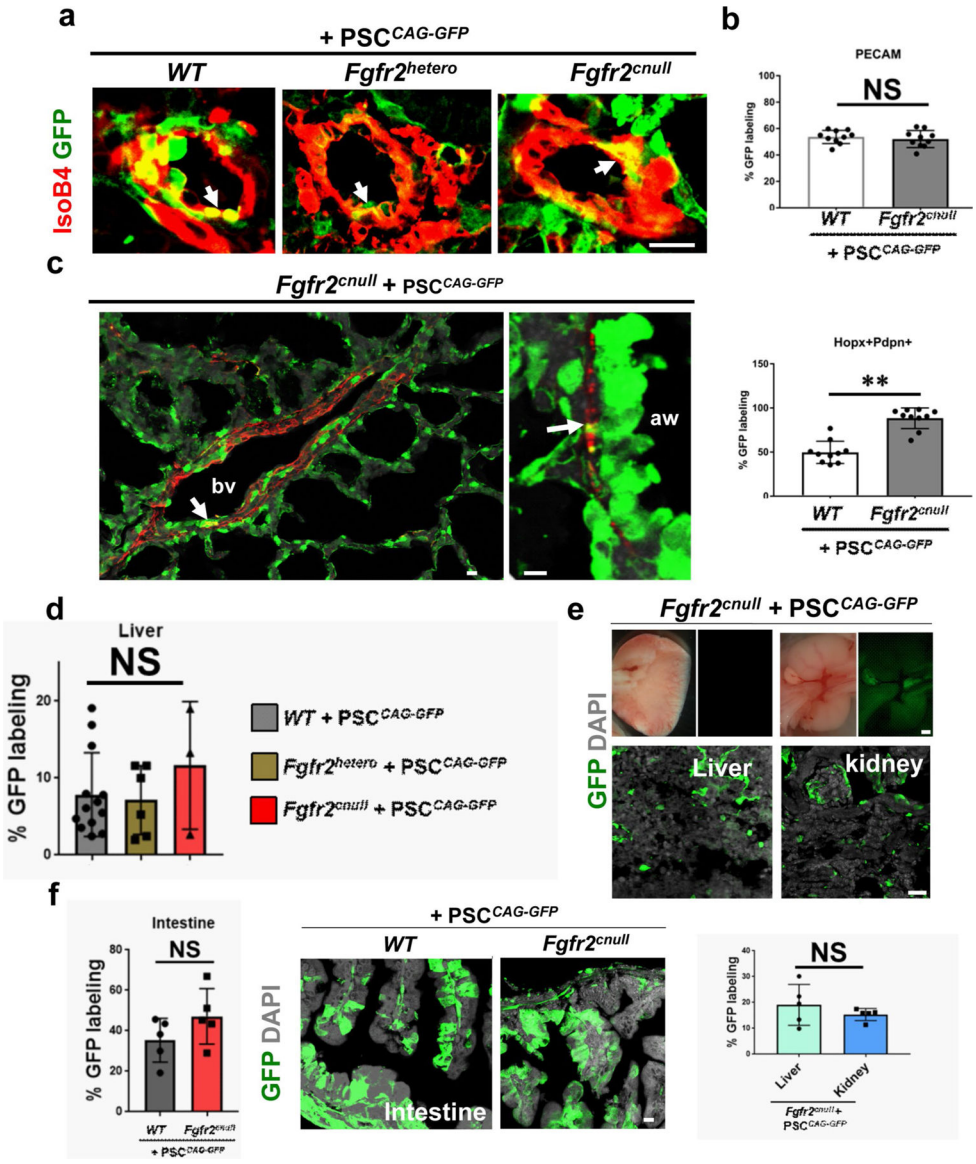

Extended Data Fig. 5 |. Chimerism in the lung alveolar vascular compartment (a–c) and extrapulmonary organs of animals complemented with VPA/LiF-treated PSC$^{CAG–GFP}$ (d–f). **a**, Immunofluorescence and confocal imaging of newborn (P0) WT + PSC$^{CAG–GFP}$, *Fgfr2*^{hetero} + PSC$^{CAG–GFP}$ and *Fgfr2*^{cnull} + PSC$^{CAG–GFP}$ chimeric lungs. Representative image of blood vessels showing GFP-Isolectin B4 double-labeled endothelial cells (arrows). **b**, Percentage of GFP labeling in endothelial (top) and alveolar type I (bottom) cells in P0 WT + PSC$^{CAG–GFP}$ and *Fgfr2*^{cnull} + PSC$^{CAG–GFP}$ chimeric lungs as determined by morphometric analysis of sections immunostained with Pecam (top) or Hopx and Pdpn (bottom). Graphs: mean ± s.e.m. of measurements in ten non-overlapping random fields per group (see also Supplementary Fig. 2 and Methods). **c**, GFP-Sma double-labeling of smooth muscle cells (arrow) in blood vessels (bv) and airways (aw) by immunofluorescence of P0

lungs from PSC$^{CAG–GFP}$ complemented *Fgfr2*^{cnull} mice. **d**, Proportion of GFP+ cells in the liver from E15.5 and P0 chimeric mice isolated by FACS. Graph represents mean ± s.e.m. of PSC$^{CAG–GFP}$-complemented WT, *Fgfr2*^{hetero} *or Fgfr2*^{cnull} animals (n = 13, 6, 3 animals, respectively). **e**, Representative images of GFP expression in liver (left) and kidney (right) from P0 *Fgfr2*^{cnull} + PSC$^{CAG–GFP}$ (whole-mount and histological sections) and quantitative analysis (bottom) of GFP labeling; graph: mean ± s.e.m. of % GFP+ cells per field in 5 random fields per group. **f**, Representative images of GFP expression in the intestine from WT or *Fgfr2*^{cnull} injected with PSC$^{CAG–GFP}$ (histological sections) and graph showing % GFP + (mean ± s.e.m., 5 random fields per 5 per group). Statistical analysis (**b**,**d**–**f**): Student's t-test; $^{**}P < 0.01$, NS: statistically non-significant. Scale bars: **a**, **b** = 10 μm, 5 μm, respectively; **e**: top panel: 20 μm, bottom panel: 1 mm; **f**: 10 μm.

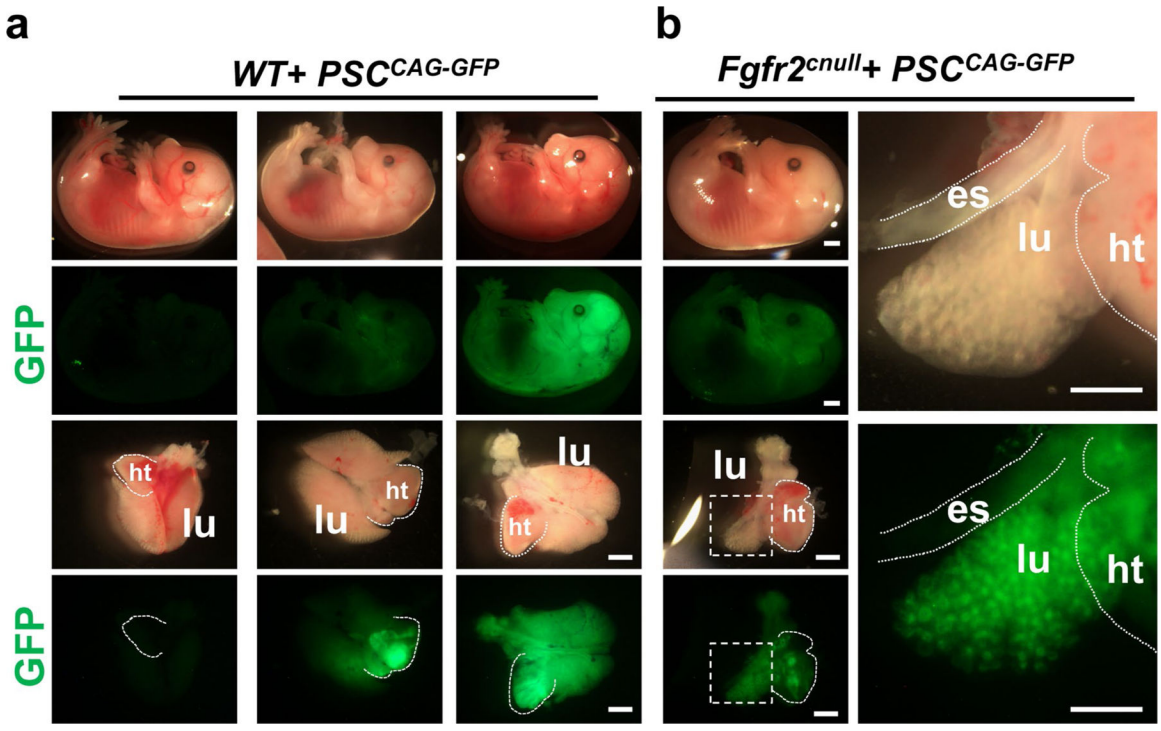

Extended Data Fig. 6 |. Low chimerism in VPA/LiF-treated PSCs$^{CAG–GFP}$ *Fgfr2*^{cnull} embryos and defective lung organogenesis.

GFP expression in whole-mount E15.5 embryos and tissues. **a**, Variable chimerism in E15.5 WT + PSCs$^{CAG–GFP}$ embryos with different levels of GFP signals in the skin, lung (lu) and heart (ht: outlined). **b**, Unilateral rescue of the lung (boxed) in E15.5 *Fgfr2*^{cnull} embryos complemented with VPA/LIF PSCs$^{CAG–GFP}$; note low chimerism in the esophagus (es) and heart. Scale bars: 1 mm.

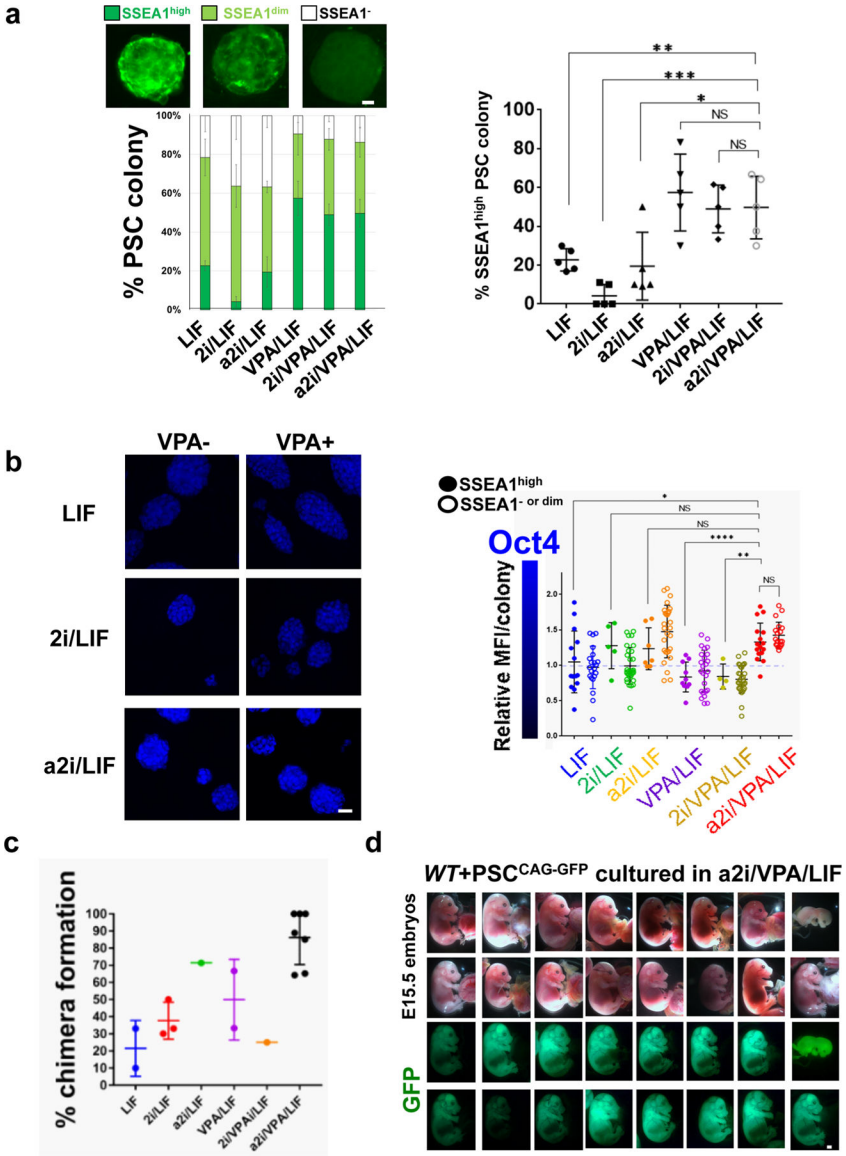

Extended Data Fig. 7 |. Comparative effects of a2i/VPA/LiF with other culture conditions in PSC pluripotency and chimerism.

a, Immunofluorescence and quantitative analysis of Ssea1 expression in PSC$^{CAG-–GFP}$ colonies in the various media tested. Top panel, representative images of Ssea1^{high}, Ssea1^{dim} and Ssea1^{negative} colonies. Bottom panel, graphs showing the percent of Ssea1-expressing colonies high, dim or negative as above (left) and percent of Ssea1^{high} colonies (right) in each culture condition. Data are mean ± s.e.m of the number of colonies per field in five non-overlapping random fields per condition. **b**, IF of Oct4 and SSEA1in PSC$^{CAG–GFP}$ cultured in the conditions indicated. Left: representative image of Oct4 staining. Right: Graph showing Oct4 expression levels in SSEA1^{high} (dots) or Ssea1 dim/negative pooled (empty dots) PSC colonies cultured as indicated. Mean fluorescent intensity (MFI) of Oct4 as assessed by imaging of 35 random colonies per culture condition (ImageJ). Relative MFI per colony shown as the Oct4 MFI of each colony normalized by the average fluorescent intensity of the PSCs cultured in LIF condition. Graphs in **a** and **b** depicting

the VPA's ability to enrich for Ssea1^{high} PSCs and the a2i/VPA/LIF effect in enhancing Oct4 expression but no significant difference in Oct4 levels between Ssea1^{high} and Ssea1^{dim} a2i/VPA/LIF-treated PSCs. **c**, Percentage of chimera formation as determined by analysis of skin/coat color in pups at P0 from blastocysts injected with PSCs cultured in each condition and transferred to foster mothers. Graph represents mean ± s.e.m. of the percentage of chimeric pups generated from the PSCs indicated (number of experiments represented by each point in the graph, see Methods). **d**) Whole-mount brightfield and GFP images of E15.5 embryos showing the high frequency of GFP-expressing chimera formation from WT hosts injected with a2i/VPA/LIF-treated PSC$^{CAG–GFP}$ (see also Table 1). Statistical analysis: one-way ANOVA (**a**,**b**) and Student's *t*-test (**c**); differences considered statistically significant if $*P < 0.05$, $**P < 0.01$, $***P < 0.001$, $****P < 0.0001$, NS: non-significant. Scale bars: **a**, **b**, **d** = 10 μm, 20 μm, 1 mm respectively.

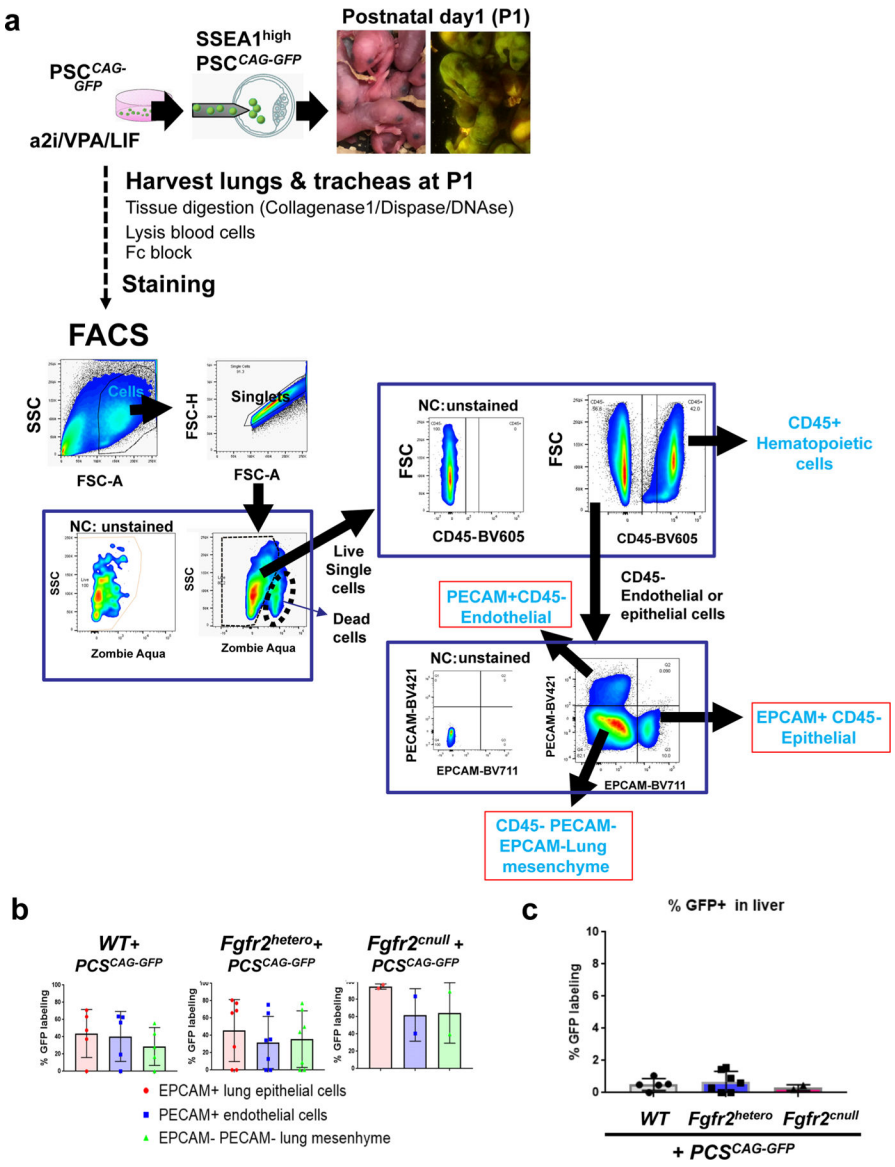

Extended Data Fig. 8 |. FACS-based assessment of cell type-specific chimerism in lung and liver from a2i/VPA/LiF -treated Ssea1^{high} PSC$^{CAG-GFP}$ WT, *Fgfr2*^{hetero}, or *Fgfr2*^{cnull} hosts. **a**, Schematics of the CBC approach (Ssea1^{high} a2i/VPA/LIF-treated PSC donor cells injected into blastocysts hosts, chimeric pups identified at birth), tissue isolation/dissociation and gating strategy for flow cytometry (FACS) analysis of different cell types in the lung. Lung cells (FSC/SCC panels) and singlets (FSC-H/FSC-A) were selected. Within the lung singlets, live cells were gated as an unstained negative control (NC) and hematopoietic (CD45+ versus CD45^{-}). In the CD45^{-} gate, we separated epithelial (Epcam+), endothelial (Pecam+) and other non-endothelial lung mesenchymal cells (Pecam/Epcam double negative). The percentage of GFP+ cells was calculated based on the unstained WT negative control gate. **b**, FACS analysis of complemented lungs (left panels) and liver (right panel) from Ssea1^{high} a2i/VPA/LIF -treated PSC$^{CAG–GFP}$ + WT (n = 5) *Fgfr2*^{hetero} (n = 7) or *Fgfr2*^{cnull} (n = 2) animals showing the percentage of GFP labeling in lung (epithelial, endothelial or non-endothelial lung mesenchymal) cells and liver. Graphs (mean ± s.e.m) depicting GFP labeling in nearly all lung epithelial cells from *Fgfr2*^{cnull} compared to heterozygous and WT, inconsistent variable labeling in lung endothelial/mesenchymal cells and low proportion of GFP+ cells in liver regardless of the genotype.

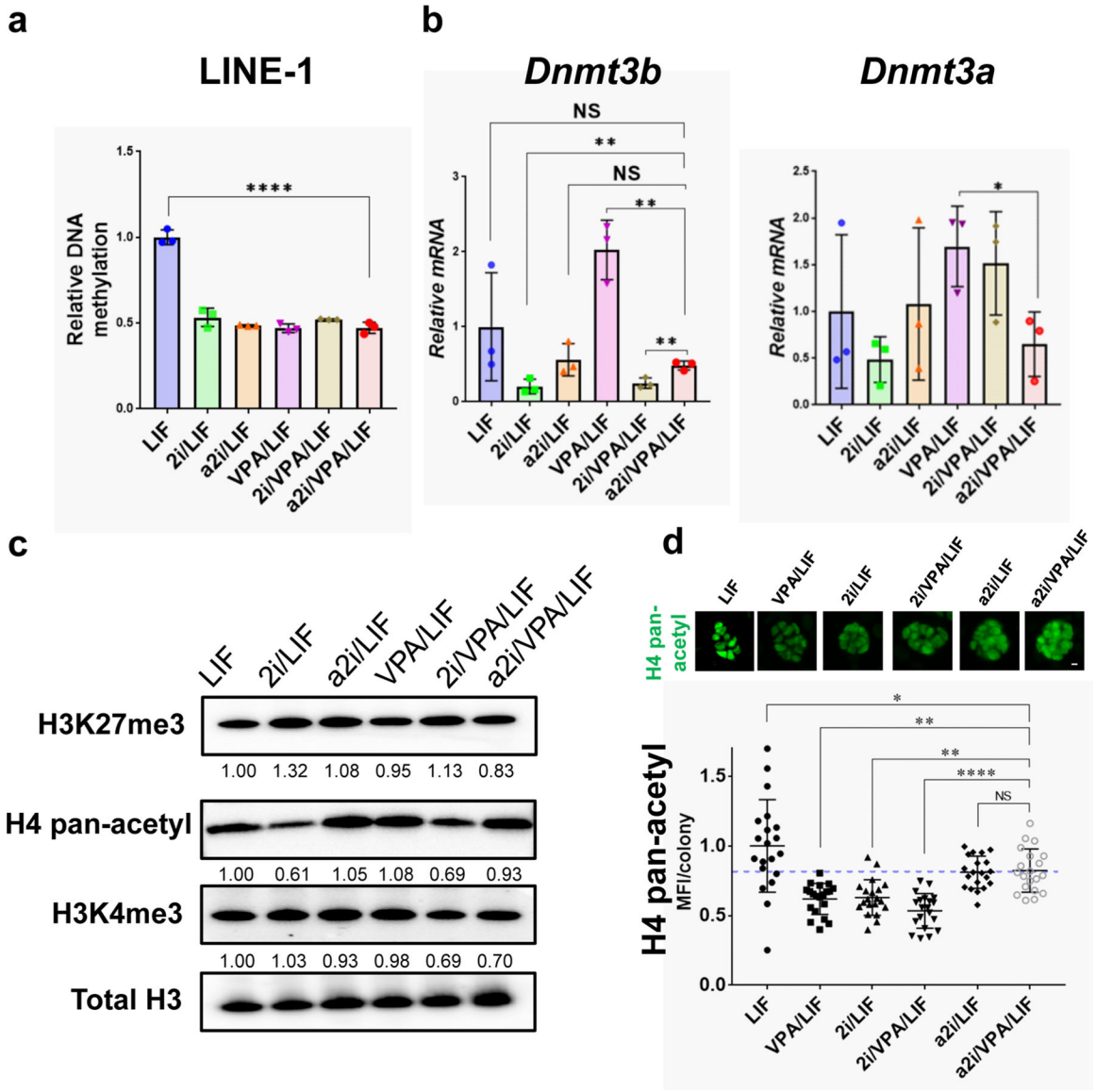

Extended Data Fig. 9 |. Effect of culture conditions in global DNA methylation, DNA methyltransferase gene expression and the patterns of histone modifications by PSC$^{CAG–GFP}$.

a, Analysis of 5-mC levels of Line-1 repeats in cell homogenates from PSC$^{CAG–GFP}$ cultures in the conditions indicated (n = 3 independent experiments); graph represents mean ± s.e.m. showing significantly lower levels of relative DNA methylation in all conditions compared to LIF. **b**, Relative levels expression of *Dnmt3b* and *Dnmt3*a in PSC$^{CAG–GFP}$ cultures by qPCR analysis; data were normalized by the LIF averaged values and represented as mean ± s.e.m (n = 3 independent experiments). **c**, Western blot of histone methyltransferases and acetylase from PSCs homogenates (n = 3 per condition); expression levels quantitated by densitometry analyses and normalized by LIF values. **d**, Immunofluorescence of histone H4ac in the PSC-treated cultures indicated (top: representative images). Mean fluorescent intensity (MFI) per colony as assessed by imaging of 20 random colonies per condition, 5 random fields (ImageJ). Graph (bottom) depicting mean ± s.e.m of MFI confirm the consistently high levels of H4-pan-acetyl expression in a2i/VPA/LIF also seen in

Western blots. Statistical analyses: one-way ANOVA (**a**,**b**) and unpaired Student's *t*-test (**d**), significance at $*P < 0.05$, $**P < 0.01$, $****P < 0.0001$, NS: non-significant.

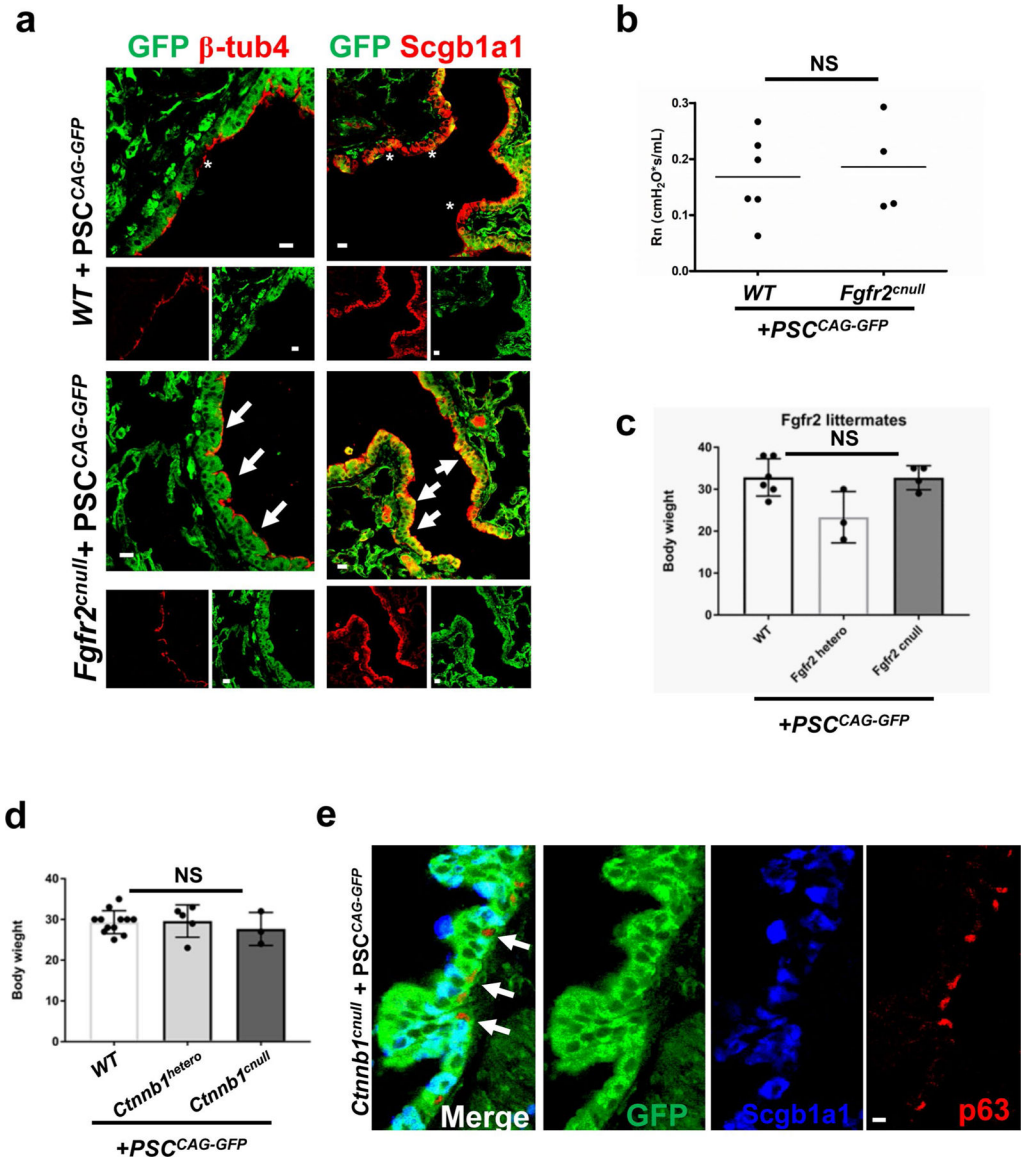

Extended Data Fig. 10 |. Normal growth, differentiation and function of adult lungs from complemented a2i/VPA/LiF-treated PSC$^{CAG–GFP}$ mature animals (see also Figs. 2 and 3).
a, Representative immunofluorescence confocal imaging of P80 a2i/VPA/LIF-treated PSC$^{CAG–GFP}$ *Fgfr2*^{cnull} and control WT + PSC$^{CAG–GFP}$ lungs double-labeled with GFP and airway differentiation markers multiciliated (β-tubulin4) and secretory (Scgb1a1) cells. Arrows: strong GFP overlapping signals in *Fgfr2*^{cnull} mutants, contrasting with the less prominent signals (* asterisks) in WT; lower panels: single-channel images. **b**, Flexivent analysis of pulmonary function in CBC-complemented day 80 WT ($n = 6$) and *Fgfr2*^{cnull} ($n = 4$); graph (mean ± s.e.m) showing non-significant (NS) difference in the resistance of conducting airways (Rn). **c**,**d**, Analysis of body weight in a2i/VPA/LIF PSC$^{CAG–GFP}$ complemented day 80 WT ($n = 6$), *Fgfr2*^{hetero} ($n = 3$), *Fgfr2*^{cnull} ($n = 4$) animals (**c**),

and day 50 WT ($n = 12$), *Ctnnb1*^{hetero} ($n = 5$), *Ctnnb1*^{cnull} ($n = 3$) animals (**d**). Graph (mean ± s.e.m) indicating no significant difference in body weight between genotypes in both *Fgfr2* and *Ctnnb1* models. **e**, IF of day50 a2i/VPA/LIF-treated PSC$^{CAG–GFP}$ + *Ctnnb1*^{cnull} lungs ($n = 3$). Representative image of GFP double labeling with markers of secretory (Scgb1a1) or basal (p63) cells in adult airways (arrows: depicts strong GFP staining contrasting). Statistical analyses: Student's *t*-test (**b**), one-way ANOVA (**c**,**d**); NS: statistically non-significant: $P > 0.05$. Scale bars: **a**,**e** = 10 μm, 5 μm, respectively.

Supplementary Material

Refer to Web version on PubMed Central for supplementary material.

Acknowledgements

We thank J. Qian, J. Huang, A. Kuforiji and M. Jiang for technical assistance, and D. Kotton and L. Oikonomou (CReM, Boston University) for invaluable reagents. We also thank the helpful scientific input from members of the Cardoso's lab and the Columbia Center for Human Development (J. Lu, H. Snoeck, S. Huang, J. Que, F. Constantini, J. Bhattacharya and M. Bacchetta) as well as from M. Morimoto (RIKEN, Japan), T. Matozaki (Kobe University), H. Masaki, S. Hamanaka (University of Tokyo) and T. Nishimura (Stanford University). We also thank K. Kennedy for help in editing the manuscript. We would like to acknowledge the support from the CCTI flow cytometry core (LSRII: NIH S10RR027050) and Columbia Stem Cell Initiative (CSCI) Flow Cytometry core (FACS Area). This work was funded by the Department of Defense, PR161857 and NIH-NHLBI 1 R01 HL148223–01 to M.M., CIRM Research Leadership Award, LA1_C12–06917 to H.N., NIH-NHLBI R35-HL135834–01 to W.V.C., Giannandrea Family Dale F. Frey Breakthrough Scientist of the Damon Runyon Foundation (DFS-28–18) and a Pew-Stewart Scholar for Cancer Research to C.L.

References

1. Murphy SL, Xu J, Kochanek KD & Arias E Mortality in the United States, 2017 NCHS Data Brief no. 328 (National Center for Health Statistics, 2018).
2. Petersen TH et al. Tissue-engineered lungs for in vivo implantation. Science 329, 538–541 (2010). [PubMed: 20576850]
3. Kotton DN & Morrisey EE Lung regeneration: mechanisms, applications and emerging stem cell populations. Nat. Med 20, 822–832 (2014). [PubMed: 25100528]
4. Matsunari H et al. Blastocyst complementation generates exogenic pancreas in vivo in apancreatic cloned pigs. Proc. Natl Acad. Sci. USA 110, 4557–4562 (2013). [PubMed: 23431169]
5. Wu J et al. Interspecies chimerism with mammalian pluripotent stem cells. Cell 168, 473–486.e15 (2017). [PubMed: 28129541]
6. Suchy F, Yamaguchi T & Nakauchi H iPSC-derived organs in vivo: challenges and promise. Cell Stem Cell 22, 21–24 (2018). [PubMed: 29304339]
7. Valapour M et al. OPTN/SRTR 2017 annual data report: lung. Am. J. Transplant 19, 404–484 (2019). [PubMed: 30811892]
8. Chen Y-W et al. A three-dimensional model of human lung development and disease from pluripotent stem cells. Nat. Cell Biol 19, 542–549 (2017). [PubMed: 28436965]
9. Dye BR et al. A bioengineered niche promotes in vivo engraftment and maturation of pluripotent stem cell derived human lung organoids. eLife 5, 1–18 (2016).
10. Ott HC et al. Regeneration and orthotopic transplantation of a bioartificial lung. Nat. Med 16, 927–933 (2010). [PubMed: 20628374]
11. Rosen C et al. Preconditioning allows engraftment of mouse and human embryonic lung cells, enabling lung repair in mice. Nat Med 21, 869–879 (2015). [PubMed: 26168294]
12. Stone KC, Mercer RR, Gehr P, Stockstill B & Crapo JD Allometric relationships of cell numbers and size in the mammalian lung. Am. J. Respir. Cell Mol. BioI 6, 235–243 (1992).

13. Crapo JD, Barry BE, Gehr P, Bachofen M & Weibel ER Cell number and cell characteristics of the normal human lung. Am. Rev. Respir. Dis 126, 332–337 (1982). [PubMed: 7103258]
14. Chen J, Lansford R, Stewart V, Young F & Alt FW RAG-2-deficient blastocyst complementation: an assay of gene function in lymphocyte development. Proc. Natl Acad. Sci. USA 90, 4528–4532 (1993). [PubMed: 8506294]
15. Kobayashi T et al. Generation of rat pancreas in mouse by interspecific blastocyst injection of pluripotent stem cells. Cell 142, 787–799 (2010). [PubMed: 20813264]
16. Yamaguchi T et al. Interspecies organogenesis generates autologous functional islets. Nature 542, 191–196 (2017). [PubMed: 28117444]
17. Usui J et al. Generation of kidney from pluripotent stem cells via blastocyst complementation. Am. J. Pathol 180, 2417–2426 (2012). [PubMed: 22507837]
18. Freedman BS Hopes and difficulties for blastocyst complementation. Nephron 139, 42–47 (2018).
19. Harris-Johnson KS, Domyan ET, Vezina CM & Sun X Beta-catenin promotes respiratory progenitor identity in mouse foregut. Proc. Natl Acad. Sci. USA 106, 16287–16292 (2009). [PubMed: 19805295]
20. Goss AM et al. Wnt2/2b and β-catenin signaling are necessary and sufficient to specify lung progenitors in the foregut. Dev. Cell 17, 290–298 (2009). [PubMed: 19686689]
21. Sekine K et al. Fgf10 is essential for limb and lung formation. Nat. Genet 21, 138–141 (1999). [PubMed: 9916808]
22. De Moerlooze L et al. An important role for the IIIb isoform of fibroblast growth factor receptor 2 (FGFR2) in mesenchymal-epithelial signalling during mouse organogenesis. Development 127, 483–492 (2000). [PubMed: 10631169]
23. Xu X et al. Fibroblast growth factor receptor 2 (FGFR2)-mediated reciprocal regulation loop between FGF8 and FGF10 is essential for limb induction. Development 125, 753–765 (1998). [PubMed: 9435295]
24. Harris KS, Zhang Z, McManus MT, Harfe BD & Sun X Dicer function is essential for lung epithelium morphogenesis. Proc. Natl Acad. Sci. USA 103, 2208–2213 (2006). [PubMed: 16452165]
25. Yu K Conditional inactivation of FGF receptor 2 reveals an essential role for FGF signaling in the regulation of osteoblast function and bone growth. Development 130, 3063–3074 (2003). [PubMed: 12756187]
26. Longmire TA et al. Efficient derivation of purified lung and thyroid progenitors from embryonic stem cells. Cell Stem Cell 10, 398–411 (2012). [PubMed: 22482505]
27. Ying QL et al. The ground state of embryonic stem cell self-renewal. Nature 453, 519–523 (2008). [PubMed: 18497825]
28. Kretsovali A, Hadjimichael C & Charmpilas N Histone deacetylase inhibitors in cell pluripotency, differentiation, and reprogramming. Stem Cells Int 2012, 184154 (2012). [PubMed: 22550500]
29. Stadtfeld M et al. Aberrant silencing of imprinted genes on chromosome 12qF1 in mouse induced pluripotent stem cells. Nature 465, 175–181 (2010). [PubMed: 20418860]
30. Choi J et al. Prolonged Mek1/2 suppression impairs the developmental potential of embryonic stem cells. Nature 548, 219–223 (2017). [PubMed: 28746311]
31. Yagi M et al. Derivation of ground-state female ES cells maintaining gamete-derived DNA methylation. Nature 548, 224–227 (2017). [PubMed: 28746308]
32. Furusawa T, Ohkoshi K, Honda C, Takahashi S & Tokunaga T Embryonic stem cells expressing both platelet endothelial cell adhesion molecule-1 and stage-specific embryonic antigen-1 differentiate predominantly into epiblast cells in a chimeric embryo1. Biol. Reprod 70, 1452–1457 (2004). [PubMed: 14736812]
33. Leitch HG et al. Naive pluripotency is associated with global DNA hypomethylation. Nat. Struct. Mol. Biol 20, 311–316 (2013). [PubMed: 23416945]
34. Lyko F The DNA methyltransferase family: a versatile toolkit for epigenetic regulation. Nat. Rev. Genet 19, 81–92 (2017). [PubMed: 29033456]

35. Brault V et al. Inactivation of the beta-catenin gene by Wnt1-Cre-mediated deletion results in dramatic brain malformation and failure of craniofacial development. Development 128, 1253–1264 (2001). [PubMed: 11262227]

36. Ke MT et al. Super-resolution mapping of neuronal circuitry with an index-optimized clearing agent. Cell Rep 14, 2718–2732 (2016). [PubMed: 26972009]

37. Mori M et al. Cytoplasmic E2f4 forms organizing centres for initiation of centriole amplification during multiciliogenesis. Nat. Commun 8, 15857 (2017). [PubMed: 28675157]

38. Huang SXL et al. The in vitro generation of lung and airway progenitor cells from human pluripotent stem cells. Nat. Protoc 10, 413–425 (2015). [PubMed: 25654758]

39. Singer XBD et al. Flow-cytometric method for simultaneous analysis of mouse lung epithelial, endothelial, and hematopoietic lineage cells. Am. J. Physiol. Lung Cell Mol. Physiol 310, L796–L801 (2016). [PubMed: 26944088]

40. Chapman HA et al. Lineage-negative progenitors mobilize to regenerate lung epithelium after major injury. Nature 517, 621–625 (2015). [PubMed: 25533958]

41. Golde WT, Gollobin P & Rodriguez LL A rapid, simple, and humane method for submandibular bleeding of mice using a lancet. Lab Anim. (NY) 34, 39–43 (2005).

42. Mori M et al. Notch3-Jagged signaling controls the pool of undifferentiated airway progenitors. Development 142, 258–267 (2015). [PubMed: 25564622]

43. Lu C et al. Histone H3K36 mutations promote sarcomagenesis through altered histone methylation landscape. Science 352, 844–849 (2016). [PubMed: 27174990]

44. Mikami M et al. Impaired relaxation of airway smooth muscle in mice lacking the actin-binding protein gelsolin. Am. J. Respir. Cell Mol. Biol 56, 628–636 (2017). [PubMed: 28118027]

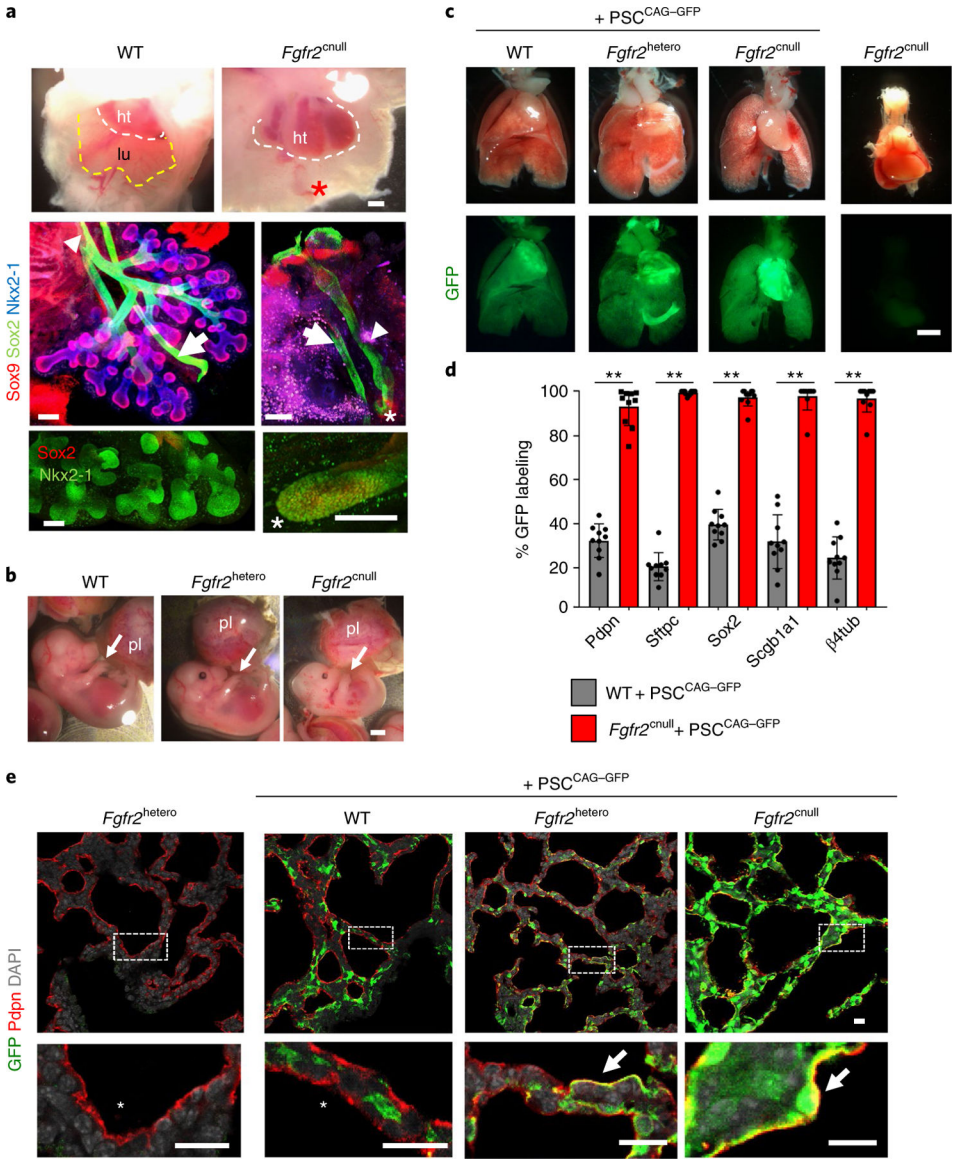

Fig. 1 |. CBC rescues lung agenesis in *Fgfr2*-deficient mice.

a, Imaging of WT and homozygous *Fgfr2*^{cnull} (*Shh*$^{cre/+}$*Fgfr2*$^{flox/flox}$) E13.5 mouse embryos. Top, whole-mount images of freshly isolated embryos. Dotted lines outline the lung (lu) and heart (Ht). An asterisk indicates the absence of lungs in *Fgfr2*^{cnull} mice. Middle, whole-mount immunofluorescence-confocal imaging of Sox2, Sox9 and Nkx2–1, depicting the esophagus (arrows) and trachea (arrowheads) in both WT (left) and *Fgfr2*^{cnull} (right) mice. Lungs are present in WT but not mutant mice (the asterisk indicates a blunt-ended trachea). Bottom, immunofluorescence imaging of Sox2 and Nkx2–1 depicts distal lung buds in WT mice, contrasting with a blunt-ended trachea in *Fgfr2*^{cnull} mice. **b**, Whole-mount images of freshly isolated E13.5 WT, *Fgfr2*^{hetero} (control heterozygous mutant *Fgfr2*: *Shh*$^{cre/+}$*Fgfr2*$^{flox/+}$) and *Fgfr2*^{cnull} embryos. Limb (arrow) and placenta (pl) are present in mice of all genotypes ($n = 5$ per group). **c**, GFP imaging of freshly isolated lungs from newborn (P0) chimeric WT, *Fgfr2*^{hetero} and *Fgfr2*^{cnull} mice, in which PSC$^{CAG–GFP}$

were used for CBC. The lung from a littermate *Fgfr2*^{cnull} mouse without PSC$^{CAG–GFP}$ injection is shown as a negative control. **d**, Quantitative analysis of GFP distribution in the indicated lung cell types by immunofluorescence co-labeling with markers of differentiation in sections of P0 lungs from WT + PSC$^{CAG–GFP}$ and *Fgfr2*^{cnull} + PSC$^{CAG–GFP}$ mice. The percentage of GFP labeling is shown in alveolar type 1 (Pdpn), type 2 (Sftpc), club (Scgb1a1) and multiciliated (β-tubulin-4) cells, or in the airway compartment regardless of cell type (Sox2). Values are shown as mean ± s.e.m. in ten random fields per sample from a representative WT and mutant lung. Student's *t*-test, $^{**}P < 0.01$. **e**, Representative confocal immunofluorescence images of GFP, Pdpn and DAPI in newborn lungs of WT, *Fgfr2*^{hetero} and *Fgfr2*^{cnull} mice complemented with VPA/LIF-treated PSC$^{CAG–GFP}$. Complementation rescued the formation of distal saccules and alveolar type 1 differentiation. *Fgfr2*^{hetero} mice without complementation were used as a negative control. Boxed areas are shown enlarged in bottom panels and depict thin-walled distal saccules (arrows indicate GFP+Pdpn+ cells; asterisk indicates GFP$^{–}$Pdpn+ cells). Scale bars, 150 μm (**a**), 2 mm (**b**), 1 mm (**c**) and 5 μm (**e**).

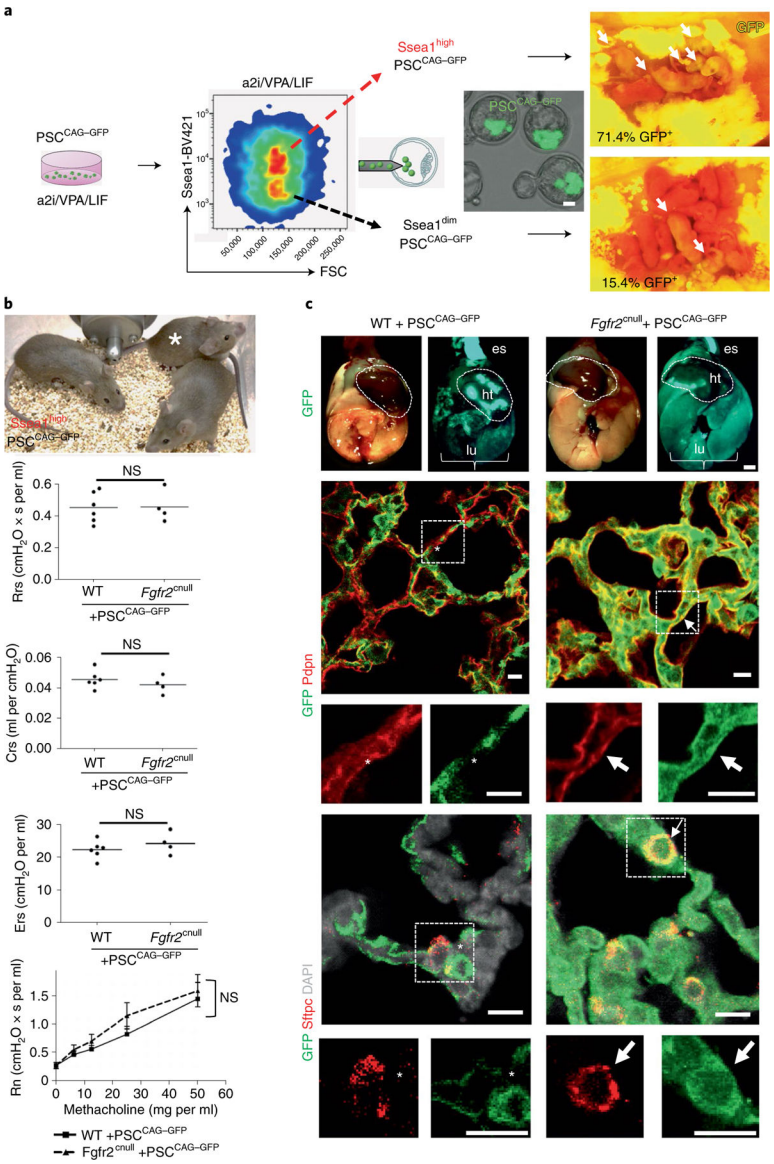

Fig. 2 |. Generation of fully functional adult lungs in *Fgfr2*-deficient mice via CBC.

a, Schematic of the experimental design: a2i/VPA/LIF-treated PSCs$^{CAG–GFP}$ were sorted into Ssea1^{high} and Ssea1^{dim} subpopulations and injected into WT blastocyst hosts, which were analyzed for chimera formation, as identified by GFP labeling in chimeric blastocysts (middle) or in the skin of chimeric P0 pups (right; arrows indicates GFP+ chimeric neonates). **b**, Top, adult *Fgfr2*^{cnull} (asterisk) and control WT littermates complemented with Ssea1^{high} PSC$^{CAG–GFP}$. Middle, resistance (Rrs), compliance (Crs) and elastance (Ers) of the respiratory system, as assessed by Flexivent analysis, in chimeric WT and *Fgfr2*^{cnull} mice. Bottom, response of lungs to increasing doses of methacholine (Rn, resistance of conducting airways). Graphs represent mean ± s.e.m. of $n = 6$ (WT) and $n = 4$ (mutant) mice per group. Student's *t*-test was used for statistical analysis. NS, statistically non-significant. **c**, Top, whole-mount GFP imaging of freshly isolated postnatal P80 adult lungs (lu), heart (ht) and esophagus (es) from *Fgfr2*^{cnull} + PSC$^{CAG–GFP}$ and littermate control

WT + $PSC^{CAG–GFP}$ mice. Brackets indicate areas where GFP staining differed between complemented control and mutant lungs. Middle, immunofluorescence images of GFP and Pdpn (a marker of alveolar type 1 cells). Bottom, immunofluorescence images of GFP and Sftpc (a marker of alveolar type 2 cells) in lung sections. Boxed areas in double-labeled images are shown as single-labeled enlarged images below (arrows, GFP+marker+ cells; asterisk, GFP^{-}marker+ cells). DAPI was used for nuclear staining. Scale bars, 10 μm (**a**), 1 mm (top, **c**) and 10 μm (middle and bottom, **c**).

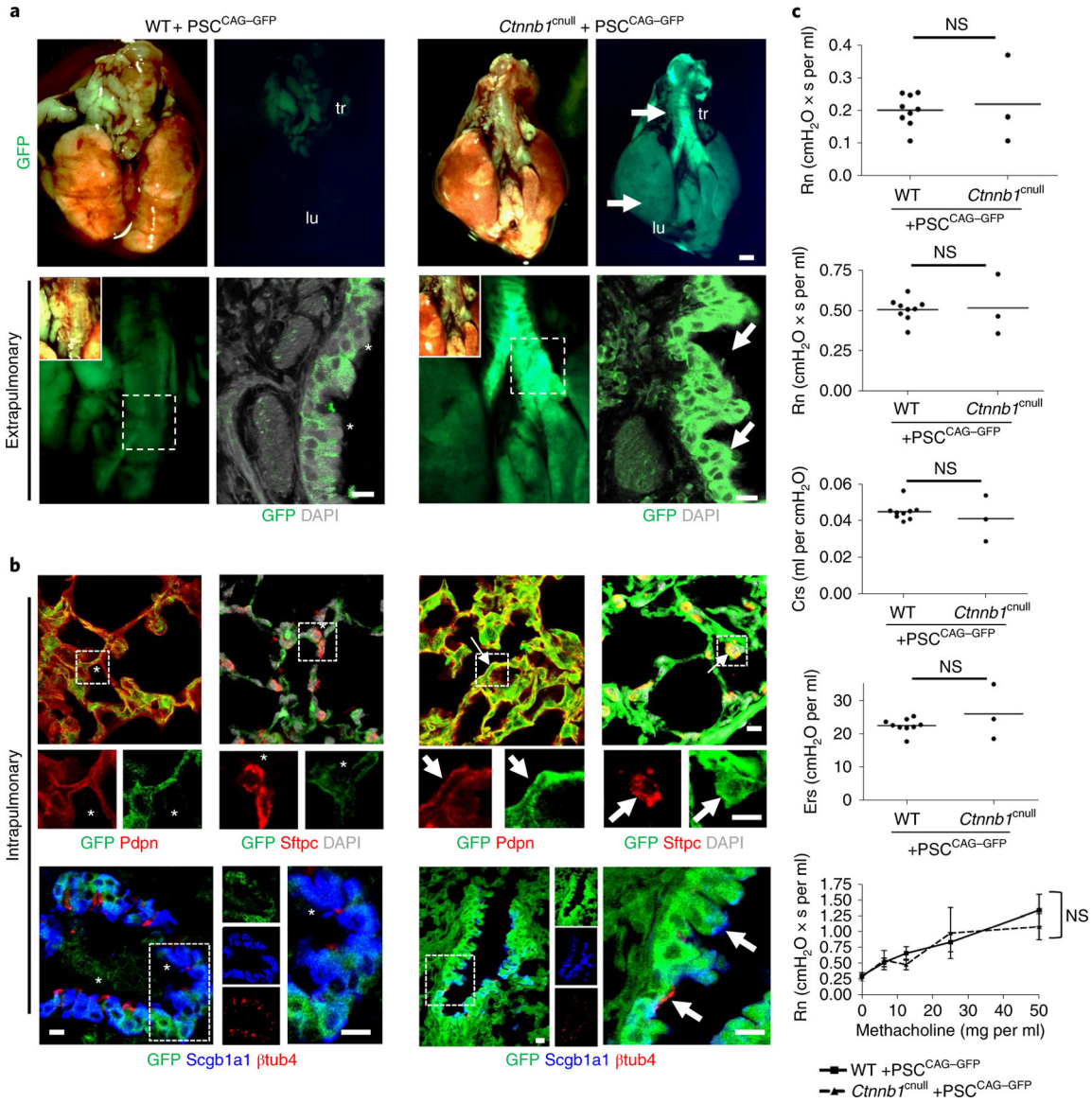

Fig. 3 |. CBC overcomes the defect in the specification of early respiratory progenitors in *Ctnnb1*-deficient mice and generates functional trachea and lungs.

a, Top, whole-mount GFP imaging of freshly isolated adult postnatal day50 complemented adult lungs (lu) and tracheas (tr) from control (WT, left) and homozygous *Ctnnb1*^{cnull} (*Shh*$^{cre/+}$*Ctnnb1*$^{flox/flox}$, right) blastocysts injected with a2i/VPA/LIF-treated PSC$^{CAG–GFP}$. Bottom, GFP imaging of whole mounts and histological sections of extrapulmonary airways (main bronchi) in WT and mutants. Boxed areas in double-labeled images are shown as single-labeled enlarged images below (arrows, GFP+ cells; asterisk, GFP$^{–}$ cells. **b**, Representative immunofluorescent staining for Pdpn, Sftpc, β-tubulin4 (βtub4) and Scgb1a1 (CC10) in the lungs of WT and mutant mice. Boxed areas in double-labeled images are shown as single-labeled enlarged images below (arrows, GFP+marker+ cells; asterisk, GFP$^{–}$ marker+ cells. DAPI was used in all panels. **c**, Resistance of conducting airways (Rn), resistance (Rrs), compliance (Crs) and elastance (Ers) of the respiratory system, as assessed by Flexivent analysis, in adult WT and *Ctnnb1*^{cnull} mice complemented with PSC$^{CAG–GFP}$.

Bottom, response of lungs to increasing doses of methacholine. A Student's *t*-test was used for statistical analysis. Graphs represent mean and standard error of n = 9 (WT), 3 (mutant) mice per group. Scale bars in (a) 1 mm (top panel), 10μm (bottom panel); (b): 10 μm.

Nat Med. Author manuscript; available in PMC 2022 June 06.

Table 1 |

Summary of PSC donor lines, culture conditions, host mouse strains and data for chimera formation, lung complementation and survival in mice subjected to CBC

Cell line	Passage number	Donor PSC background	PSC treatment	Number of host blastocysts	Host blastocyst background	Number of injected PSCs per blastocyst	% survival (number of pups or embryos/number of transferred blastocysts)	% chimera formation[a]	% complementation (number of complementation/number of chimeric animals)[b]
^{c}PSC$^{Nkx2-1-GFP}$	15	W4/129S6	2i/LIF	25	129 × B6 × CD1	10	40% (10 neonates at P0)	50% (5 chimeras)	40% (2/5) at P0 (Extended Data Fig. 1) defective complementation (*Fgfr2*^{cnull})
ES1 $^{CAG-tdTomato}$	12	C57BL/6N	LIF	40	129 × B6 × CD1	10	40% (10 neonates at P0)	10% (1 chimera)	0% (0/1) at P0 no complementation (*Fgfr2*^{cnull})
ES1 $^{CAG-tdTomato}$	14	C57BL/6N	LIF	25	129 × B6 × CD1	10	24% (6 neonates at P0)	33% (2 chimeras)	0% (0/2) at P0 no complementation (*Fgfr2*^{cnull})
ES1 $^{CAG-tdTomato}$	14	C57BL/6N	a2i/LIF	30	129 × B6 × CD1	10	23% (7 neonates at P0)	71.4% (5 chimeras)	0% (0/5) at P0 no complementation (Fgfr2 cnull)
^{c}**PSC** $^{CAG-GFP}$	10	F_1 hybrid mouse (C57BI/6 × 129)	LIF/VPA	43	129 × B6 × CD1	20	53.5% (23 neonates at P0)	66.6% (15 chimeras)	13.3% (2/15) at P0 (Fig. 1) functional complementation (*Fgfr2*^{cnull})
^{c}**PSC** $^{CAG-GFP}$	10	F_1 hybrid mouse (C57BI/6 × 129)	LIF/VPA	12	129 × B6 × CD1	20	53.5% (6 embryos at E15.5)	88% (5 chimeras)	20% (1/5) at E15.5 (Extended Data Fig. 6) defective complementation (*Fgfr2*^{cnull})
PSC $^{CAG-GFP}$	10	F_1 hybrid mouse (C57BI/6 × 129)	LIF/VPA	40	129 × B6 × CD1	20	38% (15 neonates at P0)	33.3% (5 chimeras)	0% (0/5) at P0 no complementation (*Fgfr2*^{cnull})
^{c}**PSC** $^{CAG-GFP}$	11	F_1 hybrid mouse (C57BI/6 × 129)	a2i/VPA/LIF	43	B6	20	47% (20 neonates at P0)	85% (17 chimeras)	11.8% (2/17) at P40 functional complementation (*Ctnnb1*^{cnull})
^{c}PSC$^{CAG-GFP}$	11	F_1 hybrid mouse (C57BI/6 × 129)	a2i/VPA/LIF	40	129 × B6 × CD1	20	50% (20 neonates at P0)	64.2% (13 chimeras)	30.8% (4/13) at P80 (Fig. 2) functional complementation (*Fgfr2*^{cnull})
^{c}**PSC** $^{CAG-GFP}$	11	F_1 hybrid mouse (C57BI/6 × 129)	a2i/VPA/LIF	87	B6	20	35.6% (31 neonates at P0)	65.2% (20 chimeras)	15% (3/20) at P50 (Fig. 3) functional complementation (*Ctnnb1*^{cnull})
^{c}PSC$^{CAG-GFP}$	11	F_1 hybrid mouse (C57BI/6 × 129)	a2i/VPA/LIF	18	129 × B6 × CD1	20	50% (9 embryos at E12.5)	100% (9 chimeras at E12.5)	22.22% (2/9) at E12.5 Functional

Cell line	Passage number	Donor PSC background	PSC treatment	Number of host blastocysts	Host blastocyst background	Number of injected PSCs per blastocyst	% survival (number of pups or embryos/number of transferred blastocysts)	% chimera formation[a]	% complementation (number of complementation/number of chimeric animals)[b]
									complementation (*Fgfr2*^{cnull})
[c]PSC$^{CAG-GFP}$	13	F_1 hybrid mouse (C57BI/6 × 129)	a2i/VPA/LIF	80	129 × B6 × CD1	20	25% (20 neonates at P0)	70% (14 chimeras)	14.3% (2/14) at P1 (Extended Data Fig. 8) functional complementation (*Fgfr2*^{cnull})
PSC$^{CAG-GFP}$	11	F_1 hybrid mouse (C57BI/6 × 129)	a2i/VPA/LIF	36	129 × B6 × CD1	20	44% (16 embryos at E15.5)	100% (16 chimeras at E15.5)	N.A. (Extended Data Fig. 7d)
PSC$^{CAG-GFP}$	11	F_1 hybrid mouse (C57BI/6 × 129)	a2i/VPA/LIF	51	129 × B6 × CD1	20	50% (26 neonates at P0)	88.9% (23 chimeras)	N.A.
PSC$^{CAG-GFP}$	11	F_1 hybrid mouse (C57BI/6 × 129)	a2i/VPA/LIF	35	129 × B6 × CD1	20	43% (15 neonates at P0)	100% (15 chimeras)	N.A.
CSL2J2	11	C57BL/6J C2J	2i/VPA/LIF	20	C57BL/6J	10	20% (4 neonates at P0)	25% (1 chimera)	N.A.
FL19 ARR3–1	11	C57BL/6N	a2i/VPA/LIF	20	C57BL/6J	10	60% (12 neonates at P0)	100% (12 chimeras)	N.A.
FL19 ARR3–2	11	C57BL/6N	a2i/VPA/LIF	20	C57BL/6J	10	40% (8 neonates at P0)	100% (8 chimeras)	N.A.
B7	15	C57BL/6N	2i/LIF	40	CD1	10	33% (13 neonates at P0)	62% (8 chimeras)	N.A.
SUN107.4	16	CD1	2i/LIF	20	CD1	8	30% (6 neonates at P0)	50% (3 chimeras)	N.A.

N.A., not applicable for complementation analyses, since host embryos were WT.

[a]Percentage chimera formation was based on the presence of different skin color derived from donor cells (GFP, tdTomato fluorescence or pigmentation) of P0 host neonates or embryos, as indicated.

[b]Percentage complementation was determined as the number of chimeric animals with CBC-rescued lungs in homozygous *Fgfr2*^{cnull} or *Ctnnb1*^{cnull} mutants divided by the total number of chimeric animals in the litter. The genotype of the recipient mice and figure panels containing corresponding representative images are indicated. The degree of complementation is indicated as: (1) functional complementation: CBC rescue of lungs allowed survival postnatally when examined at P0, P1 or as adults (when examined prenatally, lungs had morphological and marker expression compatible with developmental stage); (2) defective complementation: rescued lungs with developmental abnormalities (no postnatal survival); and (3) no complementation: no rescue of lung agenesis.

[c]PSCs and conditions that resulted in lung complementation.